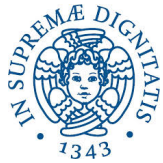


**Università di Pisa**

FACOLTÀ DI INGEGNERIA
DIPARTIMENTO DI INGEGNERIA DELL'ENERGIA E DEI SISTEMI

Corso di Dottorato in
Automatica, Robotica e Bioingegneria

SSD: ING-INF/04

Ph.D. Dissertation on

# Development and validation of haptic devices for studies on human grasp and rehabilitation

Candidate Student: **Alessandro Altobelli**

Supervisor: **Prof. Ing. Antonio Bicchi**

Course Cycle XXVII — Year of Enrolling 2011

*to my darling Chiara*
*to Sergio and Cecilia, my wonderful parents*
*to Simone, my great brother*

# Abstract

This thesis aims to develop and to validate a new set of devices for accurate investigation of human finger stiffness and force distribution in grasping tasks. The ambitious goal of this research is twofold: 1) to advance the state of art on human strategies in manipulation tasks and provide tools to assess rehabilitation procedure, 2) to investigate human strategies for impedance control that can be used for human robot interaction and control of myoelectric prosthesis.

The first part of this thesis describes two types of systems that enable to achieve a complete set of measurements on force distribution and contact point locations. More specifically, this part includes: (i) the design process and validation of tripod grasp devices with controllable stiffness at the contact to be used also for rehabilitation purposes, and (ii) the validation of multi-digit wearable sensor system. Results on devices validation as well as illustrative measurement examples are reported and discussed. The effectiveness of these devices in grasp analysis was also experimentally demonstrated and applications to neuroscientific studies are discussed.

In the second part of this thesis, the tripod devices are exploited in two different studies to investigate stiffness regulation principles in humans. The first study provides evidence on the existence of coordinated stiffening patterns in human hand fingers and establishes initial steps towards a real-time and effective modelling of finger stiffness in

tripod grasp. This pattern further supports the evidence of synergistic control in human grasping. To achieve this goal, the endpoint stiffness of the thumb, index and middle fingers of healthy subjects are experimentally identified and correlated with the electromyography (EMG) signals recorded from a dominant antagonistic pair of the forearm muscles. Our findings suggest that the magnitude of the stiffness ellipses at the fingertips grows in a coordinated way, subsequent to the co-contraction of the forearm muscles. The second study presents experimental findings on how humans modulate their hand stiffness while grasping object of varying levels of compliance. Subjects perform a grasp and lift task with a tripod-grasp object with contact surfaces of variable compliance; EMG from the main finger flexor and extensor muscles was recorded along with force and torque data at the contact points. A significant increase in the extensor muscle and cocontraction levels is evidenced with an increasing compliance at the contact points.

Overall results give solid evidence on the validity and utility of the proposed devices to investigate human grasp proprieties. The underlying motor control principles that are exploited by humans in the achievement of a reliable and robust grasp can be potentially integrated into the control framework of robotic or prosthetic hands to achieve a similar interaction performance.

# Acknowledgement

First and foremost, I would like to show my deepest gratitude to my supervisor Prof. Antonio Bicchi, whose encouragement, guidance and wide knowledge have been essential in these years and enabled me to develop in an efficient manner my research activity. It was an honor for me to have him as supervisor. Thanks to all my colleagues, friends and researchers from Interdepartmental Research Center "E. Piaggio" to support and encourage me. I would like to spend a few words for them. So let me offer my deep gratitude to Fabio Vivaldi, for his wise suggestions, Andrea Di Basco, for his encouragement and friendship, Dott. ssa Lucia Pallottino, for her guidance and patience, Dott. Ing. Marco Gabiccini, Edoardo Battaglia, Manuel G. Catalano, Edoardo Farnioli, Manolo Garabini, Alessandro Serio, Fabio Bonomo, Giorgio Grioli, for their friendship and all the help they have given to me in these years. Let me also thank Agnese Carau, Andrea Goetz, Francesca Carlino and Laura Maley for their kindness. I would like to thank all my colleagues, friends and researchers from Italian Institute of Technology, their support was fundamental to continue the work in Genova. In particular the support of Luca Colasanto, Matteo Lanfranchi, Ioannis Sarakoglou, Leonardo De Mattos, Anais Brygo, Sasha B. Godfrey and Gabriel Baud-Bovy. Finally, let me show my sincere gratitude to my friend Matteo Bianchi, for his encouragement and wise suggestions, Arash Ajoudani and Matteo Rossi, for their friendship and precious help. Obviously, a large part of my gratitude points all my "old friends" which no need to be mentioned but their support for me over these years was fundamental.

# Contents

# Introduction

The investigation of the strategies of human motor control in grasping task represent a relevant topic in neuroscience with applications in robotics. Such an investigation requires the development and the exploitation of sensing tools and devices, which are able to record all the necessary informations, for this purpose new custom devices are developed and exploited. The ambitious goal of this work is twofold: 1) to advance the state of art on human strategies in manipulation tasks and provide tools to assess rehabilitation procedure, 2) to investigate human strategies for impedance control that can be used for human robot interaction and control of myoelectric prosthesis. Despite the goal complexity requires many efforts, this thesis achieved tangible and original contributions that are suitable for robotic/prosthetic and human motor control studies.

Indeed, humans can efficiently handle disparate objects and use them in different ways. Dexterity evidenced in manipulation tasks indicates that humans have experienced advantages and disadvantages of hands through extensive practice, and they learned to make the most efficient use of interplay between available sensory information and motor capabilities. Studies and exams confirm that a large part of human cortex (Fig. 1) is dedicated to grasping and manipulation ( [7], [8], [9]), but so far human hand behaviour in grasping tasks is not completely clear. In effect, understanding the strategies adopted

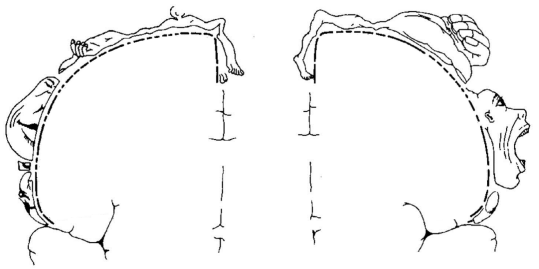

Figure 1: Human cerebral cortex: visualization of sensory functional areas and motor functional areas.

by Central Nervous System in grasping task needs to analyse the mechanical interaction between the hand and grasped object. Additionally, the presence of peripheral constrains such as physical coupling of tendons together with central neural organization leads brain to activate muscles according to "covariation" patterns, also referred to as, in a broad sense hand synergies. Recent studies confirm that, while configuration space of dexterous hands is high-dimensional, most useful grasps can be found close to a small number of discrete points. In [10], results confirm the role of first three fundamental synergies to reconstruct hand shape in pre-grasp phase. In the grasping phase

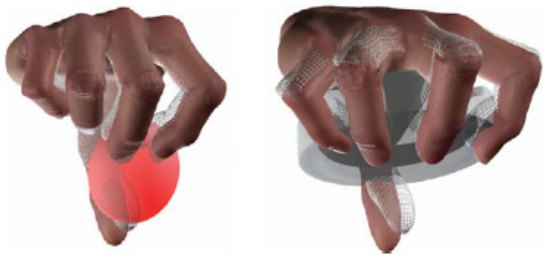

Figure 2: Application of the Soft-Synergy Model in grasping of two different objects. The reference hand (in wire frame) is achieved exploiting only the first three synergies.

understanding finger forces distribution is a challenging problem; to

study it, in [11] and [12] the authors proposed a mechanical model with synergies, called "Soft-Synergy theory" (Fig. 2). In this concept the same manipulation system with the same synergies could achieve different grasps at changing of contact point stiffness and positions.

Figure 3: The Pisa-IIT SoftHand

Despite it needs to be validated in humans, it has been already successfully used to develop an effective and adaptive robotic hand (1) able to grasp a wide number of different objects [13]. A complete analysis of human grasp includes measures and parameters that are achievable with difficulty; this represents also an important condition to validate Soft-Synergy model in human. Up to now, robotic and neuroscience studies on multi-digit grasp have focused on the control of finger forces throughout the manipulation of rigid objects at changing of different conditions (e.g. [14], [15], [16], [17]); however only few studies investigated how humans control contact forces in multi-finger grasping of deformable or soft objects [18]. Indeed, constraints and force control strategies involved in manipulating fragile or deformable objects might differ from those involved in the manipulation of rigid objects and offer new insights to the force control problem. To proceed with such investigation in a rigorous manner, what is necessary it is to develop suitable devices that are able to obtain a complete set of necessary measurements (F/T component, contact location, surface stiffness). In literature two complementary kinds of device are used to

measure them. One approach requires to build sensorized objects, by assembling parts around one or more force/torque sensors (F/T), and use them to study grasping and manipulation with a variable number of digits ( [19], [14], [20]). While this solution provides complete and reliable force/torque information, it lacks versatility for these reasons: i) it requires building a different object for every task or task condition, ii) it gives resultant centre of pressure when more than two digits are used to grasp the object (e.g. [21]).

Wearable device aims to be a complementary approach of sensorized object for human grasping studies. Common solutions use glove with several pressure sensors [22] or a set of camera to analyse the finger nail colouration [23]. Both solutions don't constrain hand posture in grasping task but lack for some aspects: the first solution doesn't allow measurement of all contact force/torque components; the second technique is limited by incapability to estimate contact point position. A challenging problem is to design and validate wearable devices that minimally constrain hand movements but allow to acquire a complete set of measurements to study the grasp.

Developing devices to study human manipulation task could be useful also to assess and improve rehabilitation therapy ( [24], [25]). More specifically these devices could allow to compare grasp proprieties between healthy subjects and patients with impaired capacity. Furthermore, these systems allow to customize therapy and increase therapeutic effectiveness of typical grasp and release exercises, in different rehabilitative scenarios, including post surgical, post trauma and post stroke rehabilitation. In recent years, technological solutions able to modulate the stiffness stand out. In [26], an "active" orthosis with variable-stiffness transducers made of dielectric elastomer was presented as a promising and viable solution for rehabilitation of patients affected by hand motor disorders. In [27] a 2 degrees-of-freedom (DOFs) end-effector based hand rehabilitation robot called the "ReHapticKnob" was evaluated and an impedance-based controller with force feedback was implemented to modulate apparent impedance of the robot end-effector.

To investigate the principle aspects previously dealt, in the first part of the thesis I developed and tested custom sensorized objects to study human motor control in grasping tasks. To allow complementary studies, I tested, also, wearable devices developed in our lab in grasp experiments. In particular the solutions with sensorized objects could have important application for rehabilitation therapy.

In the second part of the thesis, the sensorized object for grasp assessment described in the first part was used to study stiffness control in humans. The ability of humans to modulate hand stiffness when they interact with the world could also influence grasping tasks. In effect, stiffening behaviour can be realized to stabilize movement or to fix posture in isometric tasks [28]. Previous work examining finger and hand stiffness has explored various topics including the mechanical impedance of the fingers [29] or at the fingertip [30], pinch grasp stiffness during an isometric grasp task [31], or variance of stiffness depending on finger force or posture [32]. Few works study the finger stiffness when humans grasp a rigid object with three [33] or five fingers [33]; therefore the capability of Central Nervous System (CNS) to modulate the finger stiffness in multi-finger grasp is still unclear. Stiffness ellipsis at each contact could be oriented and shaped in some preferred manner that could depend by several aspects. Further hand impedance control could be affected by the grasped object stiffness. In effect, stiffening grasps with deformable object could be preferred/avoid by humans.

To investigate the aspects underlined before, I exploit the tripod devices to study: i) correlation between stiffness at fingertips and EMG signals of principal common muscles of fingers in grasping pose and ii) study how the grabbed object stiffness influences finger muscles activity in grasping task. All these works are focused to understand human grasp proprieties in depth; furthermore developed tools and methods could be proposed also to evaluate rehabilitation therapy outcomes.

## Main Research Arguments

This thesis deals about: (i) the development and testing of suitable systems for human grasping studies and (ii) studies on the control of finger stiffness in grasping tasks. These two topics are fundamental to understand the principles used by humans in motor control to interact with the external world. The developed knowledge, moreover, could be exploited in rehabilitation and prosthetic fields.

## Thesis Structure

The thesis is structured as follow:

- Chapter 1 aims to present the complexity of the human hand. It starts with a brief description of the bio mechanics model of the hand then it gives an overview on some recent hypothesis concerning the human motor control (pre-grasp, grasping force distribution, muscle activation, impedance control). Finally it points out the problem to understand the relationship between human grasp properties and stiffness at contact points.
- Chapter 2 presents two novel sensorized objects developed to study human grasp with customizable condition of stiffness at contact points.
- Chapter 3 deals with the validation of new wearable device, "ThimbleSense" developed in our lab to study grasping task with no constrains on hand posture and object shape.
- Chapter 4 presents a procedure to estimate the contact point stiffness in multi-finger grasp. A preliminary map between EMG signals and finger stiffness of hand is also reported.
- Chapter 5 investigates on the control of finger flexor/extensor muscles performed by humans, when they grasp objects with contact surfaces characterized by different levels of stiffness.

# Motivations and Contributions

The correct understanding of how human motor control pilots the hand in grasping tasks is possible only with custom devices, which give all suitable measurements to characterize such a performance. In the first part of the thesis I present two complementary devices which can be profitably used to study grasping task performed by human hand. In particular I developed two sensorized objects that could be used to investigate contact force distribution in three-digit grasping task. The devices are able to give a complete set of forces and torques exerted by each finger. Two different haptic solutions are successfully exploited to achieve different levels of stiffness at contact-points: i) Contact Area Spread Rate device to change the stiffness on-line, ii) Silicone specimen display to enable cutaneous feedback. The developed tools are also proposed to evaluate the outcomes of rehabilitation therapies.

Dealing on wearable device, I tested "ThimbleSense" system, a new tool developed in our lab to study human grasping task without hand pose constrains. I shown how the measurements collected with the device could be profitably used to perform grasp analysis exploiting robotic literature tools.

In the second part, the tripod devices are used in two works to study the stiffness control in human hand.

For the first study, I successfully integrated the sensorized object in a new set-up to estimate the cartesian stiffness of human finger in a tripod pose. This work evidenced human capability to modulate the co-contraction of the muscles to change fingertip stiffness. This study puts in evidence the importance to take in account muscle activity in grasping tasks, to have suitable values of fingertip stiffness.

In the second work, I investigated how the stiffness of grasped object could affect the control of flexion/extension activity of finger muscles. This work evidences the propensity of human to increase the finger stiffness when more compliant objects are grasped.

Chapter 1

# Human Hand Motor Control Studies

This chapter aims to give a brief overview on the complexity that is typical of hand motor control studies. Starting from biomechanical hand models to recent theories on motor control in grasping tasks, in this dissertation the important factors which affect grasp proprieties are dealt.

The mechanical structure of human hand is extremely complex and difficult to model; its rigid internal framework is made by 27 bones that are moved by 18 intrinsic muscles and 18 extrinsic muscles coupled by a network of tendons. To have a simple hand model, at least 23-24 DoFs are needed: 4 DoFs for each finger, 5 for the thumb, 1 for the radioulnar joint and 2 at the wrist. In a more detailed model, the number of DoFs increases just taking into account the hand's capability to create a palmar arch when it closes. A complete biomechanical model includes 36 muscles coupled to the bones by a complex tendons network; moreover several biomechanical constraints have to be included in the model. Joint limits or finger dimensions are clear examples of constraints which can affect the interaction of the hand with the world, and additional constraints arise from the coupling of

tendons and muscles. Some muscles span several phalanges, making it difficult to move only one joint independently; for example the flexor digitorum superficialis (FDS) and extensor digitorum comunis (EDC) muscles are divided on each finger, therefore a contraction of these muscles engages several hand joints.

Understanding how humans exploit bio-mechanics and sensory feedback of hand in everyday tasks is a challenging topic that still is not completely understood. Several studies and theories, focused on kinematic and grasping tasks have been developed. In the next section, I will give an introduction on the most recent studies which focus on important aspects of manipulation: i) Hand control in Pre-Grasp phase, ii) Grasp force distributions, iii) Muscle activations and iv) Impedance Control.

## 1.1 Hand control in Pre-grasp phase

In manipulation tasks reaching an object with the hand is not an obvious action; multiple degrees of freedom must be controlled to arrange hand shape. However, recent studies show a reduction in the number of DoFs independently controlled by the nervous system [35]. In [10], authors defined a map of postural synergies for grasping movements. In their experiments subjects grasp a large set of imagined objects, then PCA is performed with hand posture measures (Fig. 1.1 shows the synergies corresponding to the first three principal components). In this set-up, without contact between object and hand, it is possible to examine how the central nervous system plans hand posture as a function of object shape.

To grasp a real object more synergies are required to explain the hand configurations as shown in [36]. This study showed how the first three principal components described more "basic" patterns of finger motion such as hand opening/closing caused by motion at all metacarpal-phalangeal or proximal-inter phalangeal joints. Informations provided by remaining synergies could be ignored in the recon-

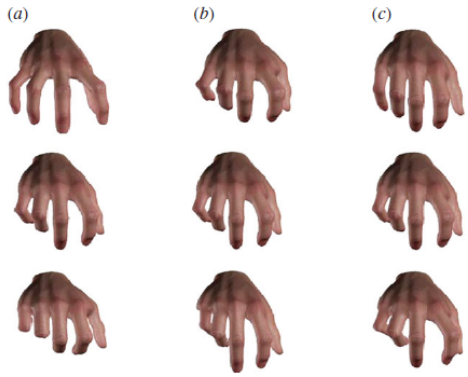


Figure 1.1: The first three postural synergies in human hand: a) first, b) second and c) third.

struction of postures. The findings suggest that few synergies could be involved to control the pre-grasp phase. This assumption could be supported by the work in [37], where synergistic finger movements are observed with transcranical magnetic stimulation (TMS) of the primary motor cortex; this behavior suggests that a modular hand muscle representation exists in human motor cortex. The CNS may be able to select the pattern of muscle activation from the identified synergies and partially involve anatomical constrains.

## 1.2 Grasp Force Distribution

To grasp and hold an object, the resultant of all forces exerted on the object has to be equal to zero. It's easy to see that an infinite number of contact force combinations could satisfy the last assertion; this topic is known in robotics as the force-close and form closure problem [38]. While this problem is partially solved in robotics; in humans it is still not clear how the CNS distribute the forces at each contact point in grasping tasks. Strategies and constraints arise in several studies that aim to understand contact force distribution in humans. For example, exerting forces only with one finger when multiple fin-

gers are in contact is impossible for humans as shown in [39], [40] and [41]. This phenomenon appears also in kinematic and is called enslaving [42]. In [19], the authors investigated the possible relation between normal forces in multi finger grasp and in [43] they showed some coordination patterns which could be task dependent. A large inter-trial variability in the normal forces exerted by each finger arise in [44]; these results, along with a coordinated action of each finger, lead authors to propose the existence of hierarchical control in manipulation action. The force modes are proposed to explain how the CNS controls the force distribution at each finger; in this theory, at each finger is linked a force pattern called force modes. Force distribution in grasping tasks could be a result of a coordinated action of force modes; however it is not clear how many degrees of freedom are exploited by the CNS because it's evident that force modes depend on the task [45] and subjects [46].

A different strategy, called the uncontrolled manifold hypothesis, arises from analysis of contact force component variability and is used to explain and quantify synergies [47]. In this theory, two classes of variables are defined: i) elemental variables related to parts of systems and ii) performance variables related to the task. This classification is used to define Bad-Variance (VB), variability of elements that could affect the precision of task, and Good-Variance (VG), variability of elements that do not affect the performance. The ratio VG/VB could identify strong synergies or weak synergies if it is large or small.

Virtual finger hypothesis is also used to explain force distribution in multi finger grasp. It asserts that one or more virtual fingers are controlled by the CNS at a high level [48]. At a lower level for each contact point, forces exerted by each finger are modulated to hold constrains of VF. In the virtual finger hypothesis, contact forces at each finger continue to be redundant and not constrained as in forces modes.

In all these theories where hierarchical control plays an important role, some variables remain unassigned. To solve the remaining redundancy optimal control theory could be used minimizing a suitable

cost function which takes into account appropriate constraints; this approach allows to find solutions that could be not compatible with humans strategies. Recent theories propose that the CNS could exploit some biological proprieties of the system to adapt itself to the task. In a grasping task, the hand could adapt itself to the grasped object exploiting finger stiffness ( [49], [11]). To explain synergies showed by humans in holding tasks, recent works [50] and [51] introduce Equilibrium Point and Reference Configuration hypothesis that assume the existence of hand configurations at which all the involved muscles would achieve zero activation levels.

## 1.3 Muscle Activity

To study human motor control, muscle activity is another factor to take into account. Each hand articulation is moved by one or more muscles with a contraction or co-contraction activity. To monitor muscle and motor unit activation, electromyographic (EMG) signals could be exploited. Focusing on the hand, which includes a large number of muscles (Fig. 1.2), EMG signal is used to investigate spatial and temporal coordination of multiple muscles in disparate tasks. The correlation analysis of EMG signals resulted in coordination patterns in muscle activation; these pattern could induce muscle synergies. This hypothesis is supported by observation of two digits force production [52], [53], three digits object hold [54], [55] and whole hand grasping [56]. In [57], focused on index finger, authors studied EMG signals of seven muscles throughout force production in several directions; finally they show high muscle correlation in the task relevant subspace instead of task irrelevant subspace. This assertion suggests that only a reduced number of muscle activation patterns are employed by the CNS. In static grasp, it is also observed that a common neural input signal at hand muscles is heterogeneously distributed across the fingers, exiting in particular extrinsic muscles instead of intrinsic muscles ( [58], [54], [55]). This finding suggests

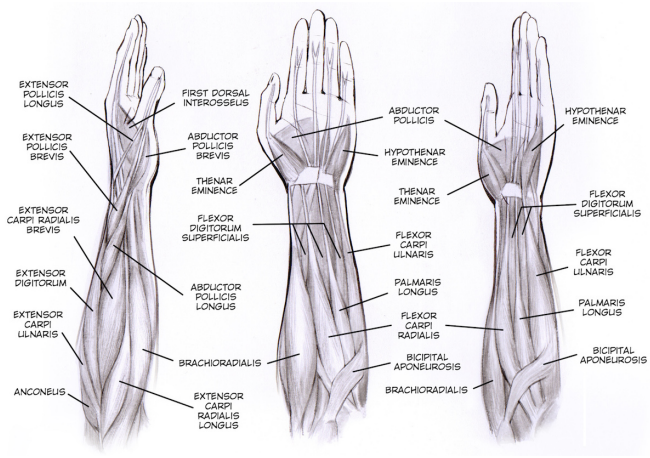


Figure 1.2: An overview of the muscles that cooperate to move human hand.

that a strong correlation lies in hand muscle activation in grasping and non-grasping tasks.

## 1.4 Impedance Control

Stability and manipulability in grasping tasks can be affected by an other import factor: the impedance at the contact point. This property relates contact forces and contact point motion. To define impedance for each contact point, two main factors must be considered: static components (stiffness) and dynamic components (damping and inertia). Although both impedance components are studied in robotics and biomechanics for the upper limb ( [59], [60], [61], [62]); only a few aspects of finger impedance have been investigated. In [30], the authors found a linear relationship between fingertip stiffness and muscle activation for the metacarpal (MCP) joint of index finger. However, when multiple joints are activated in the same finger, the previous relationship collapses and finger postures along with voluntary forces contribute to changes in the stiffness ellipsoid at finger-

tip [32].

Several additional properties on human stiffness control arise from multi finger grasp studies.

In [63], authors show a relationship between grasp stability and symmetric components of stiffness matrix in thumb-index grasp. Focusing on three digit grasp, the grasp stiffness was analysed at changing of: (i) finger position and orientation [33], as show in Fig. 1.3 and (ii) span and grasp force [64].

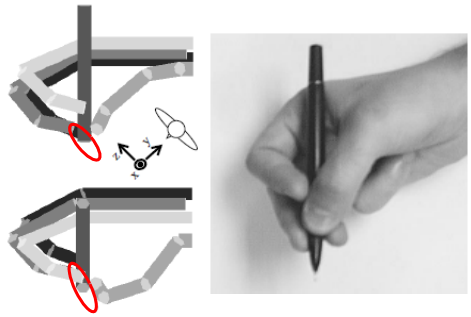

Figure 1.3: An example of grasp stiffness adopted by human during the grasp of a pen.

A possible relationship between the orientation of ellipsoids and salient task requirements results also in [65] where the authors investigate more in depth finger stiffness in grasping task of several rigid objects without restriction on contact point positions.

These results suggest that impedance control can improve performance of manipulation tasks in humans as in robot [66].

## 1.5 Outstanding Aspects in Grasping Task

Thus far, studies on multi digit grasp have focused on impedance and control of finger forces during manipulation of rigid objects. There are only a few studies that have investigated how humans grasp deformable or soft objects, despite the fact that hardness/softness is

an important characteristic of objects [67] and one of the first haptic cues which infants can use to discriminate objects and squeeze them in their hands [68]. Furthermore, the constraints and control strategies involved in manipulating fragile or deformable objects might differ from those involved in the manipulation of rigid objects. For example, avoiding large contact forces might be crucial to avoid deforming or breaking them. The grasp might also be more or less stable depending on the properties of the object. The effect of compliance when holding an object with the tripod grasp was investigated in [18] with a device where a spring was placed below each contact. The control of the contact force when holding a fragile objects with a prismatic grasp was investigated in [69] with a device that collapsed when the contact force exceeded some threshold. The role of cutaneous information (related to direct deformation of the skin) vs. kinaesthetic information (related to force indentation sensing) is an unknown aspect in grasping task; the brain uses this information to estimate stiffness at contact points but how cutaneous information influences force distribution in a grasping task remains unknown. Finally the stiffness influences the force distribution when humans grasp an object but we don't know how the motor control is affected by stiffness.

The aim of this chapter is to introduce briefly some of most important factors that influence human motor control in grasping tasks. At the same time, this description should underline the complexity that characterizes factor manifold typically involved throughout the interaction between hand and grasped object. What is noticeable from this brief description is that a better understanding of human grasp is possible only by exploiting devices able to produce a complete set of measurements; in effect, contact points, forces and torques exerted by the hand, object stiffness, and muscle activation are necessary measures to study hand-object interaction.

From an engineering point of view, two approaches are used to develop devices to study human grasp: i) sensorized objects and ii) wearable devices. The first solution requires the assembly of one or more sensors around a rigid frame; these devices allow the complete

Figure 1.4: The Grasp Perturbator [70].

Figure 1.5: The Patched Intrinsic Tactile Object [71].

Figure 1.6: The Stretchable Fingernail Sensors [72].

Figure 1.7: Tekscan Pressure Sensors [73].

Figure 1.8: Examples of sensorized objects and wearable devices to study human grasps.

measurements of force and torque at the contact point but usually they constrain hand posture. Wearable systems aim to guarantee unrestrained interaction of hand in grasping task; pressure sensor on gloves or nail color analysis are two solutions presented in literature. The limits of this approach usually are lack of contact point position and lack of complete force/torque measurements. The two approaches presented above (also referred to as "human-side" and "object-side", respectively) exhibit pros and cons, and it is difficult (if not impossible) to design a system that can fully measure the physical interaction

that occurs between hand and object throughout arbitrary manipulation tasks. It is more profitable to consider these two approaches complementary and necessary for a complete study of human grasp and rehabilitation systems.

In the first part of this thesis I propose some devices to study grasp properties following two different approaches: (i) sensorized objects and, (ii) wearable devices to measures force and torque. In the second part of this thesis, the tripod devices are exploited in two different studies to investigate stiffness regulation principles in humans. The first study provides evidence of the existence of coordinated stiffening patterns in human digits and establishes initial steps towards a real-time and effective modelling of finger stiffness in tripod grasp. The second study presents experimental findings on how humans modulate their hand stiffness while grasping objects of varying levels of compliance.

# Part I

# Devices for Human Grasp Studies

Chapter 2

# Sensorized Object approach

In this section I presented two instrumented objects designed to be grasped with three digit finger posture. Four different force/torque sensors are fixed in a profitably configuration to allow measures of contact forces exerted by each finger and the external wrench. Changing the stiffness at each contact independently is possible by two different haptic solutions. Experimental results show the validity and utility of proposed devices to investigate human grasp proprieties. As evidenced in the previus chapter these systems constrain the hand posture throughout the grasp phase but allow to measure all: i) the contact positions and ii) the force/torque components at each contact. In the next subsections, the devices are described and validated in a more detailed way.

## 2.1 Three-digit grasp haptic device with variable contact stiffness for rehabilitation and human grasping studies

In this section, I propose a device for three-digit grasp (see Fig. 2.1 and Fig. 2.2), which enables to vary the stiffness of contact points in


Figure 2.1: Three-digit grasp manipulandum.

an independent and controllable fashion, by suitably regulating the inner pressure of three pneumatic tactile displays ( [A1]). At the same time, all forces and torques acted by the user can be measured using three 6-axis Force/Torque (F/T) sensors, one for each contact point. These measurements, together with the information on finger indentation, can be used to estimate contact point location on the surface. To validate the model of the manipulandum and the correctness of the force-torque measurements, I checked that the external wrench $w_f$ derived from the three force-torque sensors placed under each finger was equivalent to the external wrench $w_e$ measured by the fourth sensor placed at the basis of the manipulandum. Apart from numerical errors, the two estimates are equal. An important skill of this device is the capability to change on line the stiffness of the contact points. This device might be profitably used for finger and hand motor and force rehabilitation as well as for studies of human grasp, e.g. to an-

alyze the effects of an abrupt change of compliance on the control of the finger forces for the simulation of a break-up of an object (e.g. when normal force exceeds some threshold). Furthermore, contact point information can be used to compute "force-focus", which is an important parameter in grasping studies with humans (see e.g. [17]). By enabling a complete force data recording, user performance can be monitored and this information used to drive an effective design of the rehabilitative therapy.

### 2.1.1 Material and methods

The three-digit grasp manipulandum was designed to be grasped with the thumb, index and middle fingers with the palm above the object, in the tripod grasp configuration (see fig. 2.1). A bubble level was attached in front of the manipulandum axis to indicate when the structure is parallel to the horizontal plane (see fig. 2.2).

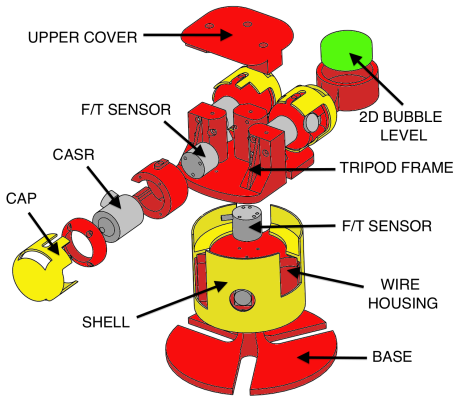


Figure 2.2: An overview of the manipulandum.

To vary the contact point stiffness in an independent and controllable fashion, three CASR (Contact Area Spread Rate) displays [74] were located under the contact surfaces. The CASR device is a pneumatic softness display that consists of a set of aluminium cylinders of

different radii, assembled in a telescopic arrangement (see fig. 2.3). For each device, a pneumatic regulator (SMC-ITV2031-21N2L4, SMC Corporation, Noblesville, IN, USA) controlled the air pressure (0.05 - 0.5 MPa) proportionally to an electrical signal (0 - 5 V) in a stepless manner. The extension (or indentation) of the device was measured with a Hall-effect sensor placed in the inner chamber of the device. A more detailed description of the CASR displays can be found in [74, 75].

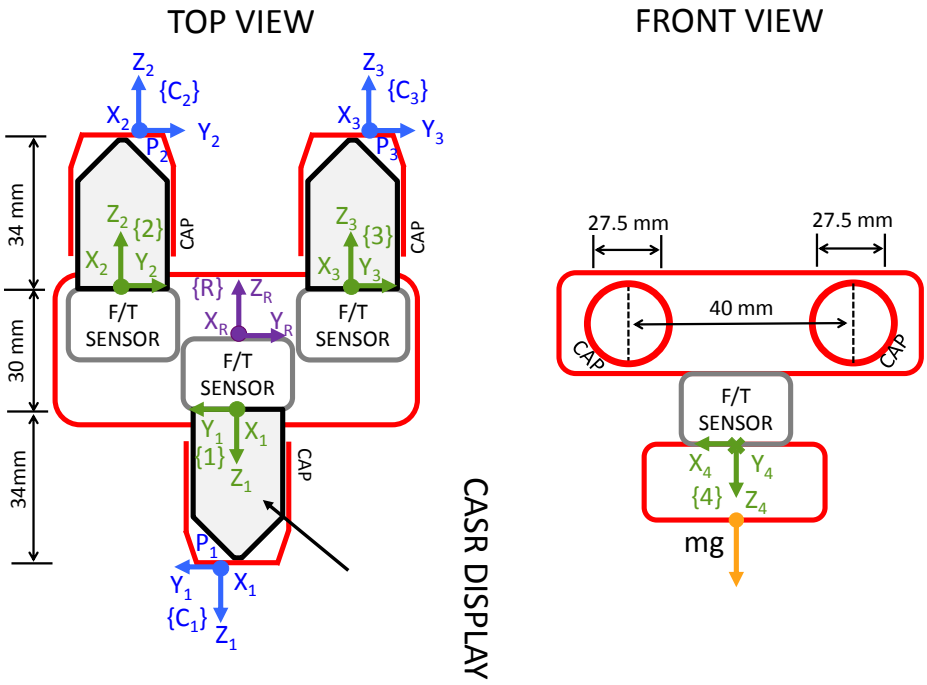


Figure 2.3: Manipulandum: sketch of the internal structure. Reference frame (purple), contact frame (blue), sensor frame (green).

Each CASR display was covered with a sliding rigid cap that was used as contact surface. The reason to use caps instead of the bare display was to reduce slippage and to avoid any "hooking" effect due to the highest CASR cylinder interacting with the soft finger pad tis-

sue. A short tube fixed to the structure guided the movement of the caps and the caps were covered with a latex sheet to increase friction. When the subject pushed against the cap/contact surface, the device displayed a reaction force correlated with the pressure, realizing the desired force-displacement relation. Each CASR display was characterized using an uni-axial testing machine "Z005 Zwick /Roell". The maximum stiffness coefficient obtainable is 5 N/mm. The stiffness range can be chosen on the basis of the rehabilitation level: the higher the stiffness, the more difficult the task. At the same time, the measurements of the contact forces can be exploited to assess patient performance and be used to eventually drive the design of further steps in therapy.

As previously mentioned, three force-torque sensors (Series Nano 17 by ATI, Apex, NC, USA) were positioned below each CASR display to measure the force and torque components applied by each finger. For the sake of readability, these components are collected in ${}^{S}w = [{}^{S}f_x, {}^{S}f_y, {}^{S}f_z, {}^{S}t_x, {}^{S}t_y, {}^{S}t_z]^T$ expressed w.r.t system of reference $S$ with $S = 1, 2, 3$ for thumb, index and middle finger, respectively (see fig. 2.3).

The total weight of the manipulandum, including the sensor cables and pneumatic valves, was 353 g. It can be easily changed to 400 g and 600 g by adding two external weights at the basis of the structure. The weight of the manipulandum can be used as a second degree of freedom to control the complexity of the task and hence set the rehabilitation level. A fourth force/torque sensor placed at the basis of the structure provides an independent measure of the weight of the manipulandum and external wrench, when the object is lifted.

The position of the contact point ${}^{S}P \in \mathbb{R}^3$ (i.e. with components $[{}^{S}p_x, {}^{S}p_y, {}^{S}p_z]^T$) is expressed w.r.t. $S$ and depends on the indentation of the CASR device (fig. 2.4). Let $L + r_S$ be the distance between the sensor and contact surface, where $r_S$ is the indentation of the device measured by the Hall-effect sensor (range 0-6 mm) and $L$ is an offset corresponding to the fixed part of the CASR device. Using the approach described in [76], the position of the contact point can be

obtained as:

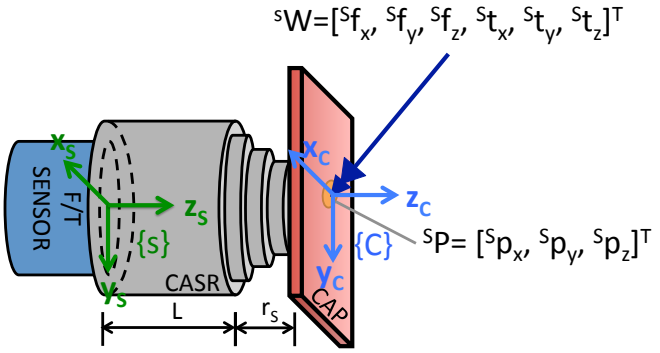


Figure 2.4: Contact point of the fingertip on the cap placed over the CASR display.

$$ {}^{S}P = \frac{({}^{S}\bar{f} \times {}^{S}t + (L + r_S) \cdot \| {}^{S}\bar{f} \| \cdot {}^{S}f)}{\| {}^{S}\bar{f} \|^2} \tag{2.1} $$

where ${}^{S}f$ and ${}^{S}t$ are the contact force and torque measured by the force-torque sensor while ${}^{S}\bar{f} = [0, 0, {}^{S}f_z]^T$. Coherently all the contact points are on the planar surface available to touch.

The contact point algorithm transports ${}^{S}f$ and ${}^{S}t$ in frame $C$, with the contact point on the cap surface (see fig. 2.4). Then forces and torques expressed in $C$ are transported in $R$ and collected in a vector $F \in \mathbb{R}^{18}$, whose components are $[{}^{R}f^i, {}^{R}t^i]$ where $i = 1, 2, 3$ refers to thumb, index and middle finger, respectively. $R$ is the reference frame placed at the center of gravity of the manipulandum (see also fig. 2.3).

The following equation relates the contact force vector $F \in \mathbb{R}^{18}$ to the external wrench $w_f \in \mathbb{R}^6$

$$ w_f = GF \tag{2.2} $$

where $G$ is the grasp matrix

$$G = \begin{pmatrix} I_3 & 0_{3\times3} & I_3 & 0_{3\times3} & I_3 & 0_{3\times3} \\ s({}^1P) & I_3 & s({}^2P) & I_3 & s({}^3P) & I_3 \end{pmatrix}. \tag{2.3}$$

and $s({}^SP)$ is the cross-product matrix for ${}^SP$ (i.e. the skew symmetric matrix such that $s({}^SP)({}^Sf) = {}^S P \times ({}^Sf)$).

When the object is lifted and held stationary, the external wrench $w_f$ corresponds to the weight of the device plus the cables of the sensors and pneumatic air.

To validate the model of the manipulandum and the correctness of the force-torque measurements, I checked that the external wrench $w_f$ derived from the three force-torque sensors placed under each finger was equivalent to the external wrench $w_e$ measured by the fourth sensor placed at the basis of the manipulandum. Apart from numerical errors, the two estimates should be equal and the following relationship should be verified as it follows

$$w_e - w_f = w_e - GF = 0. \tag{2.4}$$

### 2.1.2 Validation and Results

In this section, I report some row-data obtained with two different stiffness combinations. The same subject lifts the object to achieve the equilibrium on the horizontal plane. In the first case (see fig. 2.5), the stiffness combination is: 1.4 N/mm (thumb), 1.4 N/mm (index), 4.5 N/mm (middle). In the second case (see fig. 2.7), the stiffness combination is: 4.5 N/mm (thumb), 4.5 N/mm (index), 1.4 N/mm (middle).

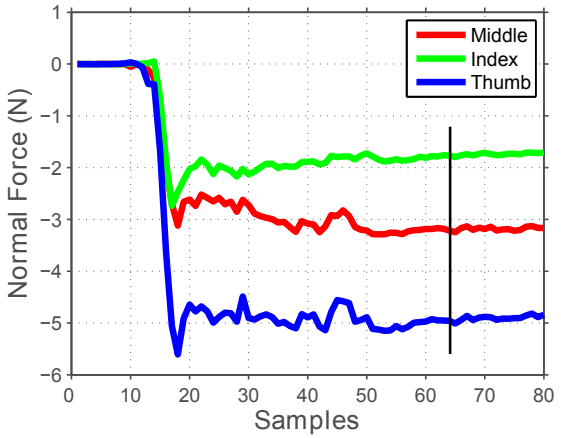


Figure 2.5: The picture shows the force distribution during the lift and hold of the manipulandum. The stiffness combination at contact points is: 1.4 N/mm (thumb), 1.4 N/mm (index), 4.5 N/mm (middle). Normal force values during the grasp. The sampling rate is 5.5 Hz. The black line splits the lift phase from the hold phase.

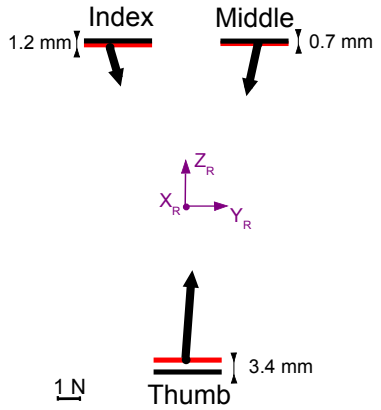


Figure 2.6: The picture shows the average of force components during the hold phase, together with finger indentation, for each finger. The stiffness combination at contact points is: 1.4 N/mm (thumb), 1.4 N/mm

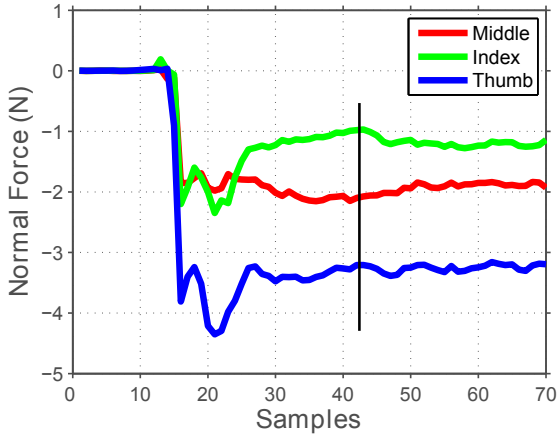


Figure 2.7: The picture shows the force distribution during the lift and hold of the manipulandum. The stiffness combination at contact points is: 4.5 N/mm (thumb), 4.5 N/mm (index), 1.4 N/mm (middle). Normal force values during the grasp. The sampling rate is 5.5 Hz. The black line splits the lift phase from the hold phase.

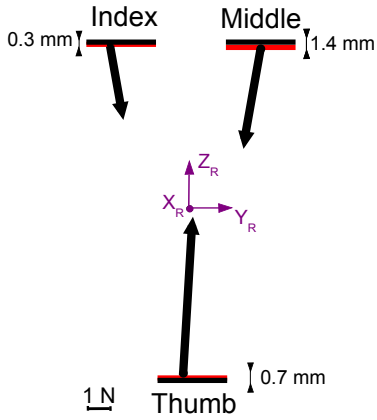


Figure 2.8: The picture shows the average of force components during the hold phase, together with finger indentation, for each finger. The stiffness combination at contact points is: 4.5 N/mm (thumb), 4.5 N/mm (index), 1.4 N/mm (middle). Average of force components during the hold phase.

To illustrate some examples of contact force measurements with different stiffness levels, I report some plots of the forces measured by the device on the horizontal plane (see figg. 2.6 and 2.8). These figures show that the position of the contact surfaces (red lines) changes as a function of the magnitude of the contact force and the stiffness displayed by the CASR device. For example, figg. 2.6 and 2.8 show the thumb forces with low and high stiffness level. Consequently the indentation decreases while the force increases.

I report also some preliminary analyses that were made to validate the device and provide some examples of contact force measurements obtained with different stiffness levels. Eight male right-handed subjects (their age ranged from 20 to 30) gave informed consent to participate in the study. No subjects reported physical limitations, such as nerve injury or finger trauma. All data collected in this study was approved by the University of Pisa Ethical Committee. Subjects were asked to grasp the manipulandum (that was leaning on a horizontal plane) with their right hand, using a tripod grasp, lift it (about 10-15 cm), and hold it until the measurement was achieved. The measurement took about 5 seconds and it started when the subject reached the grasp equilibrium position using the bubble level. After this phase, subjects re-allocated the device on the table and they came back again to the rest position.

| Comb. | T. Stiff.(N/mm) | I. Stiff. (N/mm) | M. Stiff. (N/mm) |
|---|---|---|---|
| A | 1.4 (low) | 1.4 (low) | 1.5 (low) |
| B | 1.4 (low) | 1.4 (low) | 4.5 (high) |
| C | 1.4 (low) | 4.5 (high) | 1.4 (low) |
| D | 1.4 (low) | 4.5 (high) | 4.5 (high) |
| E | 4.5 (high) | 1.4 (low) | 1.4 (low) |
| F | 4.5 (high) | 4.5 (high) | 1.4 (low) |
| G | 4.5 (high) | 1.4 (low) | 4.5 (high) |
| H | 4.5 (high) | 4.5 (high) | 4.5 (high) |

Table 2.1: Stiffness combinations.

There were eight experimental conditions, which corresponded to different combinations of stiffness levels (1.4 N/mm and 4.5 N/mm) at each contact point (see table 2.1). Subjects lifted the object 10 times for each stiffness combination for an overall number 80 trials. The sequence of trials was randomized each time.

To validate the correctness of the manipulandum model and measurements, I verified whether equation (2.4) was satisfied. Figg. 2.9 and 2.10 report the differences between the two independent estimates of the external wrench averaged across trials and subjects for each condition. The equilibrium equation is satisfied with average error values for the force components less than 0.06 N and 4 N mm for the torque components. These results validate the reliability of the measures of the device.

In this section I have presented an haptic system that is able to vary the stiffness of the contact points in an independent and controllable fashion, by suitably regulating the inner pressure of three pneumatic tactile displays. At the same time, the contact forces exerted by users in tripod grasp experiments were measured and used to estimate the contact point. Results analysis validates the correctness of the measurements in different stiffness conditions.

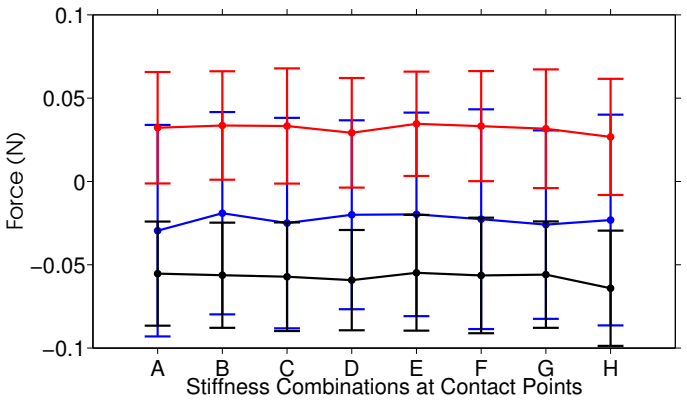


Figure 2.9: The plot shows force error component (mean ± standard deviation) behaviour along the x-axis (red), the y-axis (blue) and the z-axis (black) w.r.t. reference frame R.

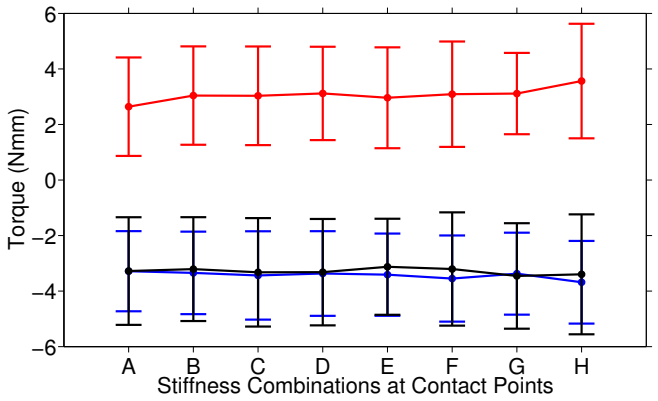


Figure 2.10: The plot shows torque error component (mean ± standard deviation) behaviour around the x-axis (red), the y-axis (blue) and the z-axis (black) w.r.t. reference frame R.

## 2.2 An instrumented manipulandum for human grasping studies

In this work [A2], I propose a modular manipulandum to be used in tripod grasp studies (see also 2.12), where the contacts can be easily changed thanks to a mechanical system. Compare to the previous work this device provides some new skill: (i) contact surface with more degree of freedom, (ii) a compensation of force/torque offsets and estimation of the mass and center of mass of the device, for different orientations and configurations in the workspace, (iii) different stiffness properties for the contact points, i.e. rigid, compliant non-deformable and compliant deformable, thus allowing to study the effects of cutaneous cues in multi-fingered grasps.

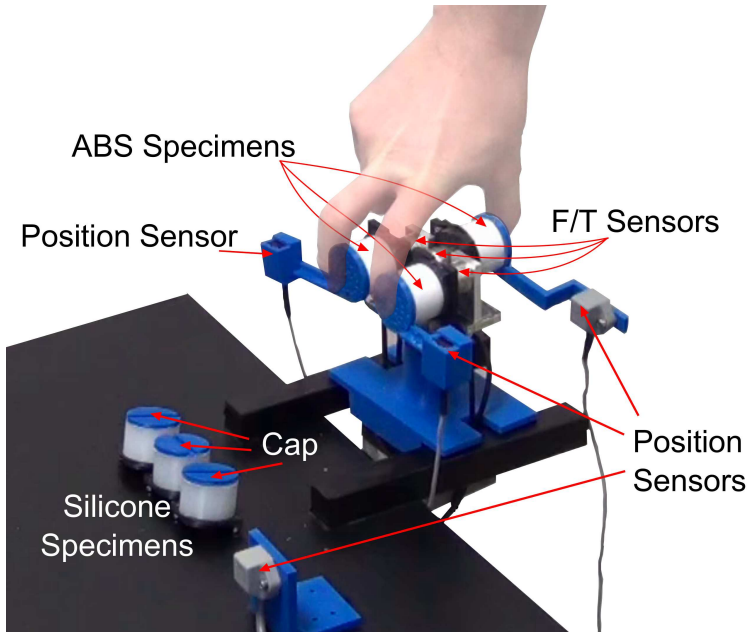


Figure 2.11: The manipulandum with its main features.

These contacts can be rigid or consist of silicone specimens. The

latter ones can be covered with a rigid surface, thus enabling contact point estimation using the algorithms and techniques reported in [76] and the integration with a motion capture system to estimate surface orientation. Indeed, in this case, where the surface can assume different orientations, contact point estimation would be not possible only using F/T measurements. Without the rigid cap, users can interact with a naturalistically deformable surface, thus enabling a proper usage of cutaneous information for grip control, while F/T quantities were recorded. Furthermore, the ease to change the contact modules and the modularity of the architecture can be used to increase/modify the number of contacts. Additionally, I suitably exploited the techniques reported in [77], [78] to define a procedure to handle F/T sensor offsets and to estimate the inertial parameters of the device (w.r.t. the local frame of each force sensor) in static conditions, i.e. the mass and the coordinates of the center of mass. In this manner the manipulandum can be profitably used for grasping experiments in any arbitrary configuration, since it allows to correctly define contact force/torque and external wrench components and to obtain reliable force measurements. In this work I first describe the mechanical design of the manipulandum and report and validate the contact point detection techniques. The effect of a correct estimation of the F/T offset and inertial parameters on contact point determination is then analyzed in different manipulandum orientations and applied forces. Finally, the effectiveness of the here reported approach is shown in some grasps experiments, where the device is held in various orientations, while the residual errors between the external wrench and the measured contact forces through the estimated grasp matrix are computed.

### 2.2.1 Material and methods

The instrumented manipulandum includes three contact surfaces which can be grasped with a tripod layout. In our experiments, the thumb in opposition to the index and middle finger were used to grasp the

manipulandum, palm down. Each contact surface consists of a contact module that can be easily attached/detacched to/from the structure of the manipulandum, through an interface engineered in ABS rapid prototyping material. The structure of the manipulandum was fabricated in aluminium using CNC (Computer Numerical Control) machine to ensure structural rigidity.

Each contact module consists of a cylindrical base in ABS (rigid case, Young Modulus 1.4 GPa) or silicone. The silicone was obtained by mixing a given quantity of a commercial bicomponent, room temperature-curing silicone (BJB TC-5005A/B), with a percentage of plasticizer (BJB TC-5005C), acting as a softener of 20%. The Young modulus of the silicone is 510 kPa [79]. By changing the percentage of plasticizer, the stiffness of the contact also changes.

The contact modules can come endowed with a rigid cap in ABS, where the receiver of the Polhemus magnetic system [1] (Colchester, VT -US) is attached trough a rigid arm/support. The emitter is placed on the bottom part of the manipulandum. In this manner, the position and orientation of the cap surface can be measured w.r.t. the emitter frame $\{E\}$. An additional receiver is attached to the table where the manipulandum is placed in rest conditions see fig. 2.11. In this manner, an inertial reference frame $\{0\}$ can be defined. For further details please refer to fig. 2.20.

Three force-torque sensor (Series Nano 17 by ATI, Apex, NC, USA) were positioned below the interface where the contact modules are attached/detached to measure the force and torque components applied by each finger.

In this manner three experimental conditions can be set: (i) rigid (ABS module, w or w/o rigid cap); (ii) compliant non-deformable (silicone with rigid cap); (iii) compliant deformable (silicone w/o rigid cap). In condition (iii) only the F/T components can be estimated, since the algorithm used for contact point detection in [76] requires information on surface orientation, which can not be achieved without

[1] The static accuracy of the Polhemus system, in terms of Root Mean Square Error (RMS) is $0.03\,in \cong 0.762\,mm$ for the position and $0.15°$ for the orientation

Polhemus system. Future works will be devoted to find a manner to estimate contact surface orientation also in this case, for example through Finite Element (FE) modeling.

The total weight of the manipulandum, including the sensor cables, is around 540 g, but it might be easily varied. A fourth F/T sensor placed at the basis of the structure provides an independent measure of the weight of the manipulandum and external wrench, when the object is lifted.

An exploded drawing view of the manipulandum with dimensions is reported in fig. 2.12.

All the systems are integrated and synchronized in Simulink (Matlab R2012a) with Simulink Block for Real Time Execution and each acquisition is performed at 100 Hz.

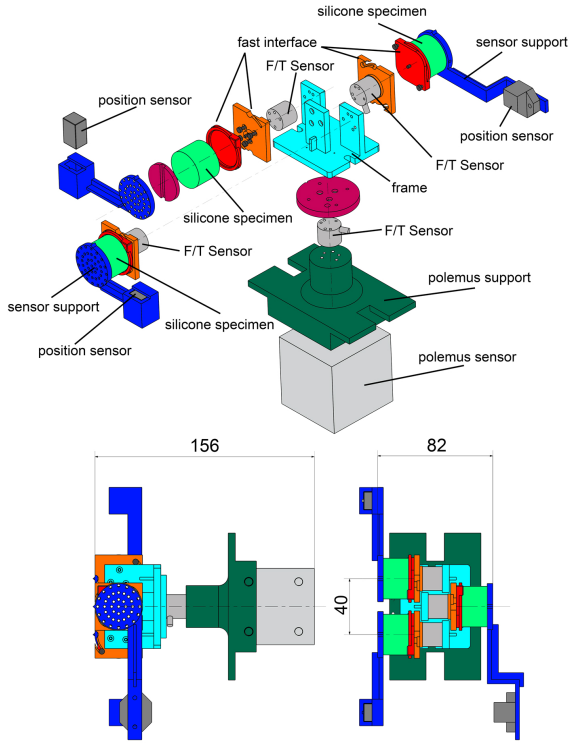


Figure 2.12: Exploded drawing view of the manipulandum and its main features with dimensions in [mm].

### 2.2.2 Contact Point Estimation

In order to estimate fingertip contact points on the tripod during grasp tasks, I use the Intrinsic Tactile Sensing Algorithm (ITSA, for more details see also [71] and [76]). Briefly, the ITSA can compute contact points from F/T measurements and from the knowledge of the shape equation of the surfaces fixed on the F/T sensor (see fig. 2.13). For the sake of clarity, here, I recall the ITSA for a single tactile surface of the tripod considering that the algorithm can be easily replicated for all the contact surfaces. The position of the contact point ${}^S c \in \mathbb{R}^3$ (i.e. with components $[{}^S c_x, {}^S c_y, {}^S c_z]^T$) is expressed w.r.t. force sensor

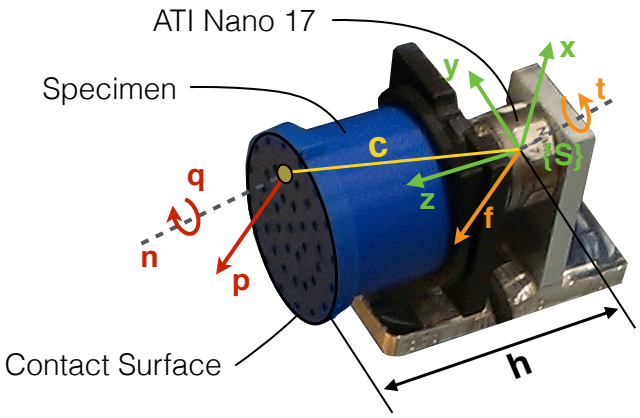


Figure 2.13: Application of the Intrinsic Tactile Sensing Algorithm (ITSA) on a contact surface of the tripod. Main features for the contact point detection are highlighted.

reference frame $\{S\}$. Let $h \in \mathbb{R}^3$ (with components $[h_x, h_y, h_z]^T$) be the offset of the surface fixed on the F/T sensor, achievable via Polhemus measurements. The position of the contact point can be obtained as:

$$ {}^{S}c = \frac{({}^{S}\bar{f} \times {}^{S}t + h \parallel {}^{S}\bar{f} \parallel {}^{S}f)}{\parallel {}^{S}\bar{f} \parallel^2} \tag{2.5} $$

where ${}^{S}f \in \mathbb{R}^3$ and ${}^{S}t \in \mathbb{R}^3$ are the contact force and torque measured by the force-torque sensor while ${}^{S}\bar{f} = [0, 0, {}^{S}f_z]^T$. Coherently all the contact points are on the planar surface available to touch. It is possible to notice that the ITSA not only detects the contact point but also computes its related forces $p \in \mathbb{R}^3$, torques $q \in \mathbb{R}^3$ and contact normal $n \in \mathbb{R}^3$ (see also fig. 2.13 for more details). For measurement homogeneity, for each contact surface, after the application of the ITSA and, thus, the detection of the contact point, sensor frame was transported $\{S\}$ into the inertial frame $\{0\}$ .

### 2.2.3 F/T Compensation

In order to achieve reliable F/T measurements, it is important to handle and compensate the offsets that can corrupt the estimation results. Although different factors (e.g. temperature) can determine it, such an offset is mainly due to the wrench exerted on the sensor by the part of the manipulandum attached on it, i.e. the part of manipulandum placed on the top of the sensor (like an object attached to the end-effector of a manipulator, where the sensor is the end-effector) and which would provide non-zero measurements even in the rest conditions.

Usually, this problem is solved by zeroing the sensor in a known configuration before each acquisition. However, when the manipulandum is arbitrarily placed in space, it is important to estimate the mass and the center of mass coordinates (the latter ones are not invariant w.r.t. translation and rotation) of the structure attached to the sensor, to enable a correct offset compensation. To properly handle these problems, I suitably implemented and applied the techniques described in [77, 78]. To do this, I collected F/T measurements in a large number of manipulandum configurations (larger than 3000) in the workspace, while the reference system of the sensors $\{S\}$ (whose position w.r.t. the receiver sensor is known) can be computed w.r.t.the inertial one from the Polhemus measurements.

For the fourth sensor, the estimation procedure will lead to the identification of the components of the external wrench that will be used in the grasp equation. In our case, this estimation is conducted in static conditions, i.e. the inertial parameters are zero, except for the mass and the center of mass of the part of the manipulandum attached to the sensor. Without loss of generality, I report the procedure only for the fourth sensor. The parameters to be estimated are: the mass of the object attached to the sensor $m$, the center of mass coordinates ($[M_x, M_y, M_z] \in \mathbb{R}^3$) expressed in the sensor frame $\{S\}$ and the offset vector components (of force and torque) w.r.t. $\{S\}$, i.e. $[f_B, \tau_B] \in \mathbb{R}^6$. The F/T readings are collected for each i-th sample

in the external wrench vector defined as $w_i = [f_x, f_y, f_z, \tau_x, \tau_y, \tau_z]^T$ w.r.t. $\{S\}$, while the vector composed with all the unknowns is $\phi = \begin{bmatrix} m & M_x & M_y & M_z & f_B & \tau_B \end{bmatrix}^T$ w.r.t $\{S\}$. In this manner, it's possible to write:

$$w_i = \left[\begin{array}{cc|c} ({}^S R_0)(-\bar{g}) & 0^{3\times 3} & \\ 0^{3\times 1} & \wedge(({}^S R_0)(\bar{g})) & I^{6\times 6} \end{array}\right] \phi \tag{2.6}$$

where $\bar{g}$ is the gravity vector w.r.t the inertial reference frame $\{0\}$, ${}^0 R_S$ is the rotation matrix to transport $\{0\}$ into $\{S\}$ and $\wedge(\cdot)$ is the skew-operator.

For the i-th wrench recording, I can define

$$A_i = \left[\begin{array}{cc|c} ({}^0 R_S)^{-1}(-\bar{g}) & 0 & \\ 0 & \wedge(({}^S R_0)(\bar{g})) & I^{6\times 6} \end{array}\right] \tag{2.7}$$

If I collect $n$ ($n >> 1$) wrench recordings, I can define the linear system

$$W = \begin{bmatrix} w_1 \\ w_2 \\ \vdots \\ w_n \end{bmatrix} = \begin{bmatrix} A_1 \\ A_2 \\ \vdots \\ A_n \end{bmatrix} \phi = A\phi. \tag{2.8}$$

It is then possible to estimate all the unknown parameters as

$$\phi = A^{\dagger} W \tag{2.9}$$

where $\dagger$ is the Moore-Penrose pseudoinverse. Once the mass $m$ and the center of mass of the part of the manipulandum attached to the fourth sensor, i.e. above the fourth sensor, are estimated, and hence the offset of F/T measurements, it is possible to individuate

the external wrench components w.r.t. $\{0\}$. The offset-corrected F/T measurements provided by the sensor can be expressed w.r.t. the frame $\{B\}$, which is placed at the estimated center of mass. The weight in $\{B\}$ can be obtained by multiplying $m$ for the gravity vector $\bar{g}$ (expressed in $\{B\}$). Finally the weight and the measured forces can be algebraically summed and expressed in $\{0\}$. In this manner the components of the external wrench in $\{0\}$ can be obtained as well as reliable F/T readings in any workspace configuration, as it is shown in fig. 2.20.

### 2.2.4 Experiments on Contact Position

To test the accuracy of the contact point detection, we use the ABS contact surface shown in fig. 2.14 where five aluminium dowel pins (diameter 2 mm, height 0.5 mm) with known dimensions and positions w.r.t the center of the contact surface were placed. Each spike was touched 10 times with a thin tip and the ITSA was applied after F/T compensation procedure described in Section 2.3. Four different conditions are considered: $ABS_i$, $ABS_{ti}$, $SILICONE_i$, $SILICONE_{ti}$. The labels $ABS$ and $SILICONE$ indicate the materials of the contacts under the rigid ABS plate where the spikes were placed. The subscript "$i$" indicates that the manipulandum was tilted w.r.t. the horizontal plane (approximately 30°) and normal forces to the surface were applied within the range from 2 to 10 N and tangential forces were from $-1$ to 1 N; "$ti$" indicates that the manipulandum was tilted (approximately 30°) and the normal forces were from 2 to 5 N and the tangential forces were within the range from $-3$ to 3 N.

Estimated contact points are shown in figg. 2.15, 2.16, 2.17, 2.18. The error is computed as the absolute difference between the radial distance from the estimated contact point and the center of the spike and the radius of the spike. In Table 2.2, we report the error averaged across all trials and spike locations with related standard deviation for each test type. Even if the silicone case in tilted condition with large tangential forces exhibits the largest mean error, probably due

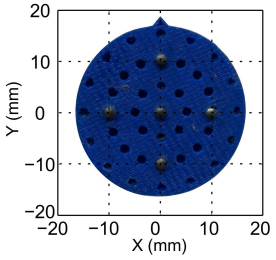


Figure 2.14: Testing plate

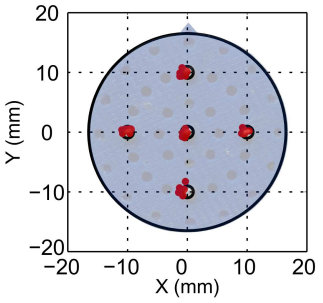


Figure 2.15: $ABS_i$

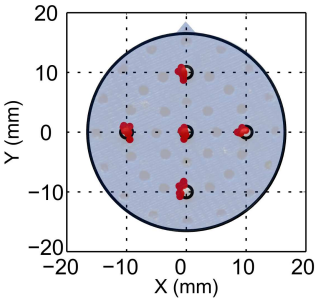


Figure 2.16: $ABS_{ti}$

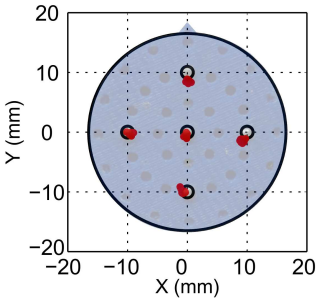


Figure 2.17: $SIL_{\cdot i}$

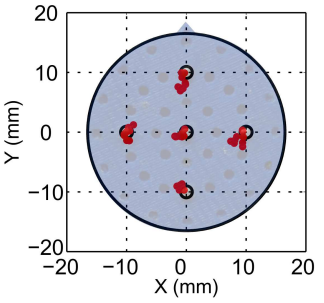


Figure 2.18: $SIL_{\cdot ti}$

Figure 2.19: ITSA contact point detection accuracy in different conditions. Red points represent contact point positions estimated by ITSA.

to a non correct coupling between the silicone surface and the ABS, the algorithm for contact point detection with F/T compensation still provides satisfactory results (the average error is under 1 mm). The results are comparable with those reported in [71].

| Tests | Mean Error | Standard Deviation |
|---|---|---|
| $ABS_i$ | 0.24 mm | 0.20 mm |
| $ABS_{ti}$ | 0.28 mm | 0.20 mm |
| $SILICONE_i$ | 0.50 mm | 0.31 mm |
| $SILICONE_{ti}$ | 0.90 mm | 0.65 mm |

Table 2.2: Estimation errors for ITSA. *ABS* and *SILICONE* refer to ABS rigid contacts and silicone contacts, respectively.

### 2.2.5 Validation On Grasping and Results

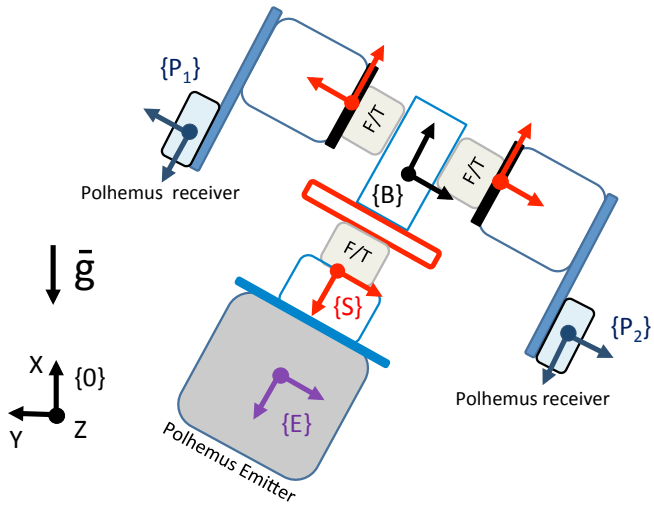


Figure 2.20: The manipulandum structure with reference frames and components reported.

To properly validated the effectiveness of the manipulandum and of the methods here described (contact point detection and F/T com-

pensation for different configuration of the device in the workspace), I compute the following equation, which relates the contact force vector $F \in \mathbb{R}^{18}$ to the external wrench $w_f \in \mathbb{R}^6$ (expressed in $\{0\}$), for different manipulandum orientation

$$w_f = GF \tag{2.10}$$

where $G$ is the grasp matrix, $^\wedge(\cdot)$ is the skew-matrix operator and $C_1$, $C_2$ and $C_3$ are the contact point calculated through ITSA and with F/T compensation

$$G = \begin{pmatrix} I_3 & 0_{3\times3} & I_3 & 0_{3\times3} & I_3 & 0_{3\times3} \\ {}^\wedge C_1 & I_3 & {}^\wedge C_2 & I_3 & {}^\wedge C_3 & I_3 \end{pmatrix}. \tag{2.11}$$

When the object is lifted and held stationary, the external wrench $w_f$ corresponds to the weight of the device plus the cables of the sensors.

To validate the model of the manipulandum and the correctness of the force-torque measurements, I checked that the external wrench $w_f$ derived from the three force-torque sensors placed under each finger was equivalent to the external wrench $w_e$ measured by the fourth sensor placed in the basis of the manipulator. Apart from numerical errors, the two estimates should be equal and the following relationship should be verified

$$w_e - w_f = w_e - GF = 0 \tag{2.12}$$

The absolute residual error is computed as : $|w_e - GF|$. I computed the absolute error for 10 different configurations of the manipulandum, with rigid and deformable compliant contacts. The absolute average errors are reported for the two conditions in Table 2.3.

In this case, errors are comparable with the one reported in [A1] and between the two contact conditions, despite the different orientations of the manipulandum, the uncertainties introduced by the

| Components | $ABS$ | $SILICONE$ |
|---|---|---|
| $f_x$ | 0.0725 ± 0.0589 | 0.0496 ± 0.0422 |
| $f_y$ | 0.0769 ± 0.0603 | 0.0470 ± 0.0408 |
| $f_z$ | 0.1150 ± 0.0738 | 0.1327 ± 0.0763 |
| $\tau_x$ | 9.7638 ± 3.4614 | 12.2726 ± 2.5275 |
| $\tau_y$ | 2.8398 ± 2.2499 | 1.8448 ± 1.4165 |
| $\tau_z$ | 3.7975 ± 2.4095 | 6.4420 ± 3.8180 |

Table 2.3: Average absolute residual error with standard deviation for different manipulandum configuration. $ABS$ and $SILICONE$ refer to ABS rigid contacts and silicone contacts, respectively. $f_x$, $f_y$, $f_z$, $\tau_x$, $\tau_y$, $\tau_z$ refer to the force and torque components w.r.t. $\{0\}$.

Polhemus and those due to the interface between the contact modules and the cap. These results validate the reliability of the here proposed techniques. A short video of device capabilities is uploaded at [B6].

In this paper I have presented a modular manipulandum that can be used to study force distribution in human grasp for tripod layouts. The device allows to independently change each of the contact modules, thus varying contact stiffness.

The manipulandum combines F/T sensing and motion tracking technology to provide a complete characterization of the contact forces and moments applied on the contact surfaces of an object in any arbitrary orientation. This work represents a great technological effort to integrate different methods and technical solutions, such as (i) the algorithm described in [76] to estimate contact point location for varying-orientation contact surfaces and (ii) the procedures described in [77, 78] to handle force/torque offsets and estimate the

mass and the center of mass of the device in different orientations. In addition, given the modularity of the architecture and the simple mechanism used to attach/detach the contact modules, this structure can be easily modified in order to study different multi-finger grasp configurations. In particular, this mechanism can be used to change easily the stiffness properties of the contact surface, thus enabling the study of the effects of cutaneous cues in human grasps.

## 2.3 Neuroscientific Studies and Applications

As noted in Chapter 1, only a few human studies have investigated the control in multi digit grasp when holding a deformable objects. The devices described here can be used to investigate different motor control issues. One of this issue is whether contact forces are directly controlled by the Central Nervous System (CNS) or if they result from the interaction between central commands from the CNS and biomechanical properties of the human hand. As demonstrated by a large number of recent studies (e.g. [13], [80]), control can be simplified by letting the fingers mold themselves around the object. However, it is still not clear how such control occurs in human grasp and the relative importance of force control and passive properties of the hand is highly debated in motor control [49]. In this respect, it is noteworthy that these devices provides a way to manipulate the contact compliance under each digit separately, which is crucial to understand interaction between digits [18]. At the same time, the devices can provides necessary information about the position of the fingertip (contact point) on the object, which is crucial in the analysis of the grasp. This fact together with the possibility to use the device [A2] in any configuration by compensating sensor offset and estimating device inertial parameters can be profitably exploited to investigate models on force control distribution, e.g. equilibrium point [51] and/or virtual finger hypothesis [16], in any arbitrary orientation of the manipulandum, thus enabling a more ecological interaction.

The manipulandum presented in [A2] also offers the possibility to investigate the contribution of different sensory cues in softness perception, when the silicone cylinders are grasped with and without a rigid cover. It has been suggested that tactile system can provide a direct information about the softness of a deformable object when it is touched with the naked fingertip. In this case, the rate of change of average pressure is invariant with respect to indentation velocity and the object stiffness might be directly encoded in the population response of SAI mechanoreceptors [81]. In contrast, when the deformable object is touched with a rigid probe or when the surface of the compliant object is rigid, it is necessary to integrate proprioceptive and tactile information. For example, stiffness might be estimated from information about the rate of force and indentation velocity provided by tactile and kineasthetic inputs.

## 2.4 Conclusions

These devices are validated and usable for neuroscientific studies on human grasp force distribution and control. This part of the thesis contributes to advance the state of the art of "object-side" approaches for force measurements and to enable the investigation of the different factors that influence human grip control. Applications in rehabilitation scenarios to assess the outcomes of rehabilitation therapies will be also evaluated. In the second part of the thesis the tripod devices are profitably used to investigate some aspects of human motor control.

Chapter 3

# Wearable approach: Thimblesense, a fingertip-wearable tactile sensor for grasp analysis

In this chapter, I tested and validated the "ThimbleSense" system (see 3.1) a new wearable individual digit force/torque sensor developed and presented by E.Battaglia in [82]. This system aims to integrate the grasp analysis achievable with tripod devices presented in the Chapter 2 where the position of the contact surfaces is fixed. ThimbleSense allows to obtain measurement of contact forces between hand and grasped objects without constrains on the hand postures. The main advantage of this approach with respect to more conventional solutions is the possibility of being versatile without losing accuracy: instead of building many sensorized objects for different experiments, it is possible to employ ThimbleSense to study grasps of a variety of objects, while still retaining the complete force/torque measurements. Unfortunately, ThimbleSense rigid shells are interposed between the fingertip and grasped object. This inevitably modifies the physiological mechanical deformation that would otherwise occur at the bare fingerpad in direct contact with objects. An experiment shows that

Figure 3.1: A ThimbleSense device.

excessive grip forces are attenuated with training as the subjects familiarizes him/herself with the ThimbleSense. This effect evidences that sensorized object and wearable object are both necessary to investigate different aspects of human grasp. In this work I briefly introduce the concept and the implementation of individual-digit wearable force/torque sensors, later I present some experiments to validate the device [A3]. In particular, my contributions in this work are: (i) to define a procedure to handle F/T sensor offsets and to estimate the inertial parameters of the device in static conditions, (ii) to validate the measures of the device with some experiments. Results evidenced that internal forces estimated with the ThimbleSense are inside the null space of the grasp matrix.

## 3.1 Concept and Implementation

In this section I briefly described the concept and the implementation of ThimbleSense Device using a generic structural mechanics problem formulation.

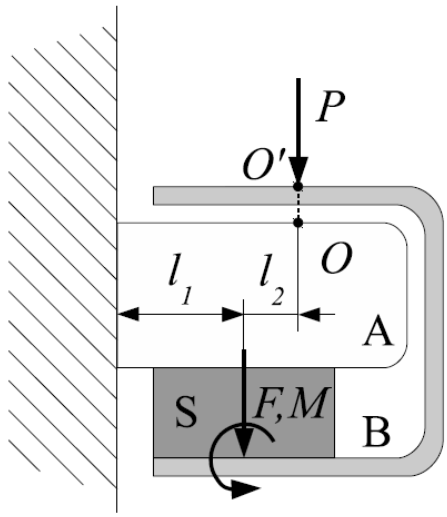


Figure 3.2: The concept of ThimbleSense.

Without loss of correctness, the mechanic system including finger and ThimbleSense can be simplified as 2D example shown in Fig. 2a. A rigid body **A**, attached to a frame, withstands a force $P$ applied on a point $O$ at position $l$, perpendicularly with respect to its main axis. Let us suppose that a sensor **S**, able to measure force F and torque M applied on its surface, is available where a force is acted on a rigid object in the point $P$. The ThimbleSense device, non-invasive to the finger, works as show in Fig. 3.2: by assembling the sensor **S** between the object **A** and a properly designed shell **B**, the system minimizes alteration to the way the load is applied. The system is developed to be placed on the finger without completely altering the grasp with interposition of a cumbersome object between the finger

and the contact.

Following this concept, a F/T sensor is assembled between an inner and an outer shell separated by a gap.

The finger finds its accomodation inside the inner shell, and once the outer shell gets in contact with an object the action applied is routed though the sensor, which constitutes the only mechanical coupling element between the two shells. Owing to this a complete measurement of forces and torques can be obtained: thus, since the geometry of the external support is known, it is possible to obtain the position of the contact centroid of the loading force $P$, through the algorithm defined in [76].

A number of factors must be taken into account to obtain a functional design, namely:

- *Size*: the device must be as small as possible, to minimize encumbrance. Consequently, all layers between finger and external surface of the outer shell must be as thin as possible; at the same time they need to be thick enough to keep the outer shell separated from the inner shell when a load is applied.

- *Weight*: the device needs to be light, to minimize the effort necessary to move it. For this reason a material with a high stiffness/weight ratio should be chosen.

- *Ergonomics*: the device must be shaped in such a way as to leave finger movements unhindered, as much as it is possible.

Overall, the grasping process should ideally be unaffected, and it should be possible to seamlessly place five devices, one on each finger, without them excessively interfering with hand movements and grasping capabilities. However, it is natural to expect that wearing a rigid shell over the finger will somehow alter the grasping process: this problem has been subject of study in [83], where it was shown that wearing a rigid shell on fingers significantly alters haptic recognition of common objects. The validation procedure presented in ( [A3]) will address this issue.

To finalize the mechanical design of the *ThimbleSense* shells, the ATI nano 17 six axis F/T sensor was selected: the sensors used in all experiments performed for this work had SI-50-0.5 calibration. To obtain a friction coefficient on the thimble shell comparable with the human skin, an artificial fingerpad built with latex and rubber was applied to the outer shell, in order to mimic the natural friction behavior of human skin. The position and the orientation of the ThimbleSense in a global reference frame $B$ are measured with a motion capture system (Phase Space, [84]). A support with four LED markers is attached to each thimble to obtain redundancy on the measurements. The algorithm in [85], is exploited to estimate the position of the thimble in the reference frame $B$. Finally all the Force and torques measured by the sensor are expressed w.r.t $B$. To achieve reliable F/T measurements, it is important to compensate the offset generated by the weight of the outer shell and LED support that can corrupt the force measurements. While in static conditions this problem is solved by zeroing the sensor before each acquisition, if the thimbles are arbitrarily placed in space it is necessary to compensate the bias on measurement, which can be done from knowledge of the mass and center of mass of the structure attached externally to the sensor by exploiting the technique described in [14] and [15]. An exploded view of the ThimbleSense and the complete set-up are shown in Figg. 3.3a and 3.3b

## 3.2 Weight Bias Compensation

To avoid measurement errors the F/T sensors need to be zeroed before each acquisition. This static zeroing cannot however take into account the bias that a body attached to the sensor induces with its weight when orientation changes. In this case it is possible to compensate for the weight-induced bias from knowledge of the mass and of the center of mass coordinates of the structure attached. In particular I used the techniques described in Section 2.3, applying it on data ac-

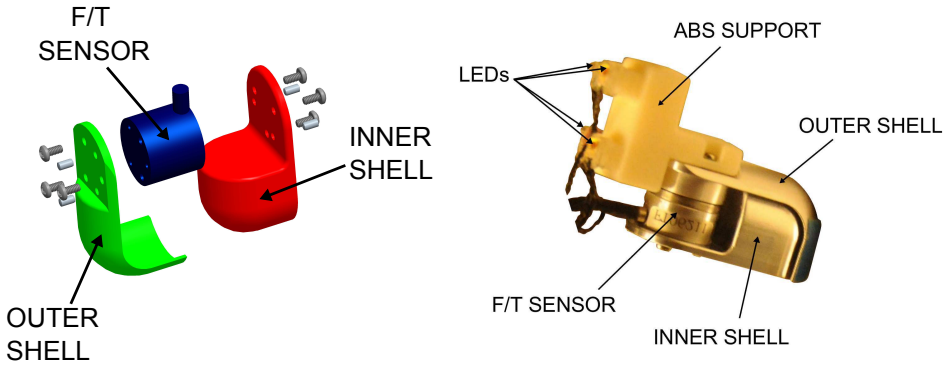


(a) Exploded view.

(b) ThimbleSense set-up.

Figure 3.3: The ThimbleSense.

quired during a motion for which the thimbles orientations were slowly changed around the whole workspace, with no object being grasped. Under these conditions the dynamic actions can be neglected and the F/T measurements collected can be ascribed only to the weight of the external shell and the ABS support.

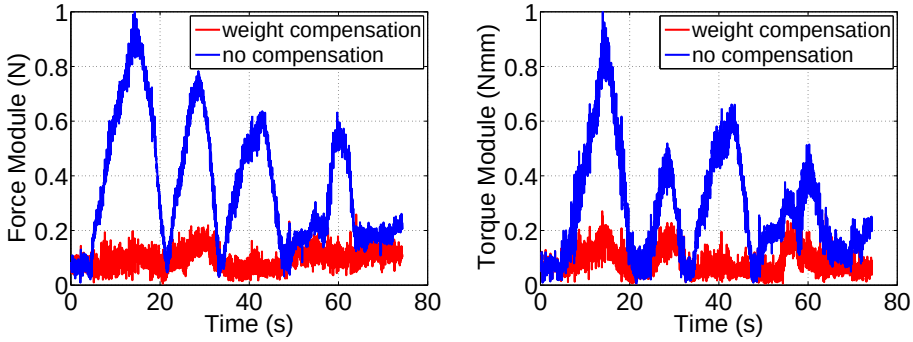


(a) Force Error

(b) Torque Error

Figure 3.4: Measurement errors during calibration with and without bias removal on Thumb.

In Fig.3.4 shows measurements of the norm of force and torque for

| | Force (N) | | Torque (Nmm) | |
|---|---|---|---|---|
| Thumb | 0.03 | 0.12 | 0.61 | 2.16 |
| Index | 0.03 | 0.09 | 0.53 | 1.84 |
| Middle | 0.03 | 0.11 | 0.69 | 2.15 |
| Ring | 0.03 | 0.11 | 0.68 | 1.95 |
| Little | 0.04 | 0.11 | 0.82 | 1.80 |

Table 3.1: RMSE for each finger during calibration: with and without weight compensation.

the thumb, with and without compensation. It can be seen that the error with respect to the expected zero value is consistently lower when weight compensation is applied. Similar results are observed for the other fingers, and application of the weight compensation produces errors that are systematically lower, as quantified numerically by the Root Mean Square Errors in Tab.3.1.

## 3.3 Validation and Results

In this section I propose a validation of the device that uses the classic robot grasping analysis [86]. A subject (male, age 27) was asked to grasp two balls of different weights while wearing ThimbleSense on fingertips. The first was a soft ball (mass $m_1 = 0.053\ Kg$, radius $R_1 = 50\ mm$) and was grasped with the whole hand (number of fingers used $n_f = 5$), while the second was a tennis ball filled tightly with iron (mass $m_2 = 0.32\ Kg$, radius $R_2 = 33\ mm$), and was grasped with four fingers ($n_f = 4$) owing to its smaller radius. In both cases the subject was instructed to lift the ball, squeeze it while holding it still with forces of different intensities, and put it down again. The

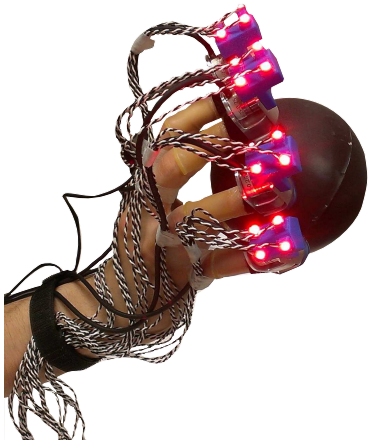

Figure 3.5: Experiment setup.

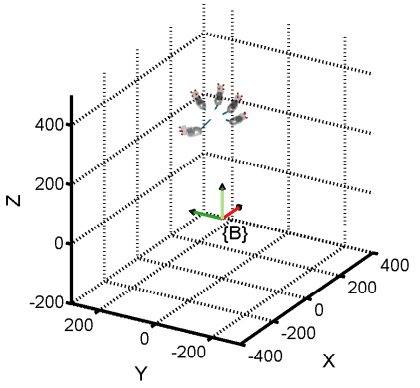


Figure 3.6: Ball grasp and reconstruction.

validation procedure consisted of two different experiments: in the first one the goal was to verify that the grasp equilibrium condition was fulfilled during the holding phase, while for the second I checked that the internal force variation was inside the null space of the grasp matrix.

### 3.3.1 Experiments 1

In this section I illustrate a procedure to verify that using $n_f$ fingers to grasp an object, the vector of measured generalized forces $\mathbf{t} \in \mathbb{R}^{6n_f}$, obtained from the fingertips measurements provided by ThimbleSenses, was correctly related to the applied external wrench $\mathbf{w} \in \mathbb{R}^6$ by the grasp equation

$$\mathbf{w} = G\mathbf{t}, \tag{3.1}$$

which should be verified under quasi-static conditions. The grasp matrix $G \in \mathbb{R}^{6\times 6n_f}$ can be written as

$$G = \begin{pmatrix} I_3 & 0_{3\times 3} & \dots & I_3 & 0_{3\times 3} \\ {}^{\wedge}\mathbf{c}_1 & I_3 & \dots & {}^{\wedge}\mathbf{c}_{n_f} & I_3 \end{pmatrix}, \tag{3.2}$$

where ${}^{\wedge}(\cdot)$ is the skew-matrix operator and $\mathbf{c}_1 \dots \mathbf{c}_{n_f}$ are the contact points coordinates calculated through the intrinsic tactile sensing algorithm, expressed in a reference system with origin in the center of mass of the ball $\mathbf{b}$ and oriented as the fixed base frame $B$.

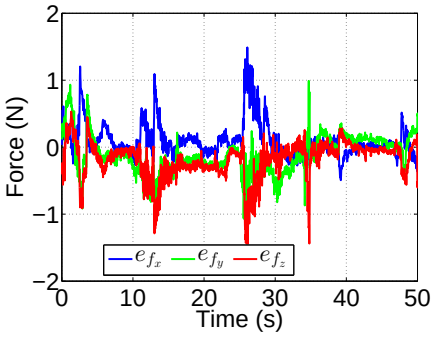


(a) Force error components.

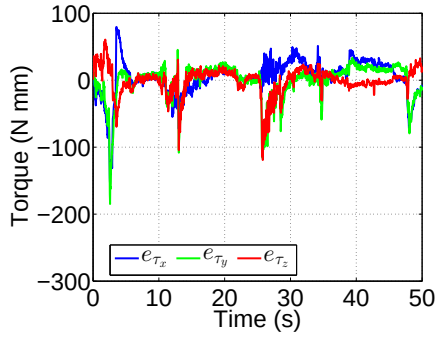


(b) Torque error components.

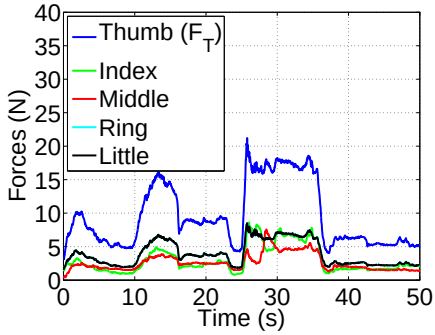


(c) Grasp analysis for the ball of mass $m_1 = 0.053Kg$.

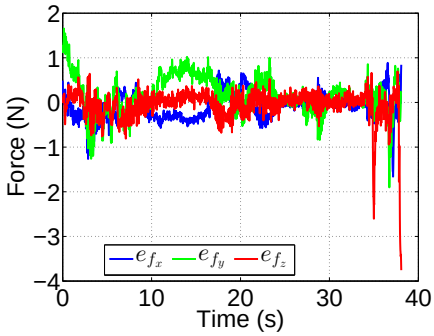


(a) Force error components.

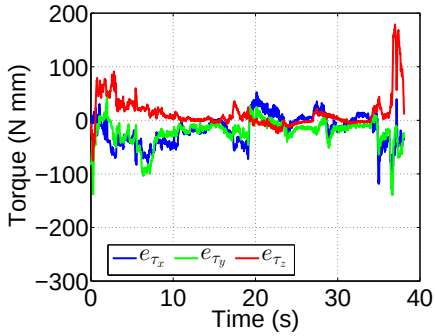


(b) Torque error components.

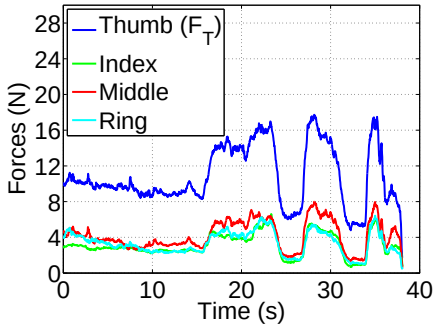


(c) Grasp analysis for the ball of mass $m_2 = 0.32Kg$.

When the ball is lifted and moved slowly, inertia actions can be neglected and the wrench $w_f$ is only influenced by the weight of the object.

Since the ball mass $m$ is known, a nominal value can be assigned for the external wrench $\mathbf{w} = \bar{\mathbf{w}} = [0, 0, -mg, 0, 0, 0]^T$, with $g = 9.81$ m/s$^2$. The residual error $\mathbf{e}$ is thus computed as

$$\mathbf{e} := \bar{\mathbf{w}} - G\mathbf{t} = \begin{bmatrix} e_{f_x} & e_{f_y} & e_{f_z} & e_{\tau_x} & e_{\tau_y} & e_{\tau_z} \end{bmatrix}^T . \tag{3.3}$$

Figures 3.8a, 3.8b, 3.8a and 3.8b show plots of the result for two trials. The following observations can be made:

- The overall grasp error tends to increase when fingertip forces

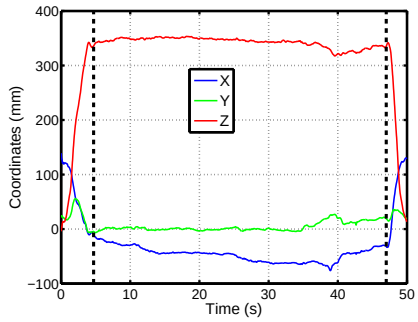


(a) Ball position **b** in space.

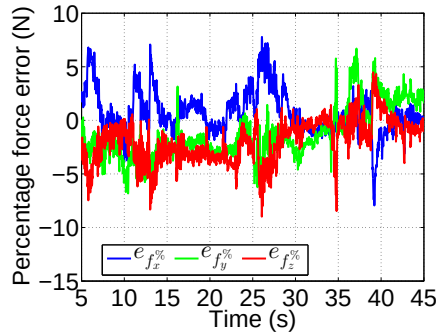


(b) Normalized force error.

Figure 3.7: Error normalization for the ball of mass $m_1 = 0.053$ Kg.

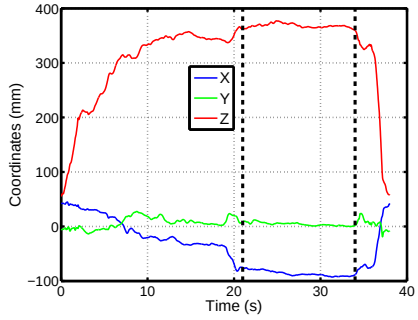


(a) Ball position **b** in space.

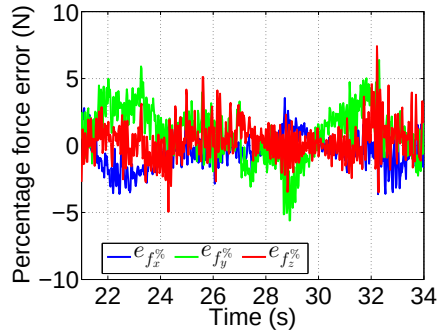


(b) Normalized force error.

Figure 3.8: Error normalization for the ball of mass $m_1 = 0.32$ Kg.

are higher;

- There is a transition at the beginning and at the end of the task where errors are relatively higher even if grasp forces are low: this is caused by the fact that, since the ball is in motion, equation (3.1) no longer holds true.

Therefore, it can be interesting to consider a force percentage er-

ror, defined as

$$\mathbf{e}_{f^{\%}} := \left[ e_{f_x^{\%}} \; e_{f_y^{\%}} \; e_{f_z^{\%}} \right] = 100 \left[ \frac{e_{f_x}}{f_T} \; \frac{e_{f_y}}{f_T} \; \frac{e_{f_z}}{f_T} \right]^T, \tag{3.4}$$

where $f_T$ is the norm of the force applied by the thumb on the object, which was chosen as indication of the intensity of grasp. The percentage error is considered for the time frame during which the ball is held still. In order to identify such time frame, I estimated the position of the ball center of mass over time. For each finger, an estimate $\mathbf{b}_i$ of the ball center can be obtained as

$$\mathbf{b}_i = \mathbf{c}_i + R\mathbf{n}_i, \tag{3.5}$$

where $R$ mm is the radius of the ball and $\mathbf{n}_i$ is the unit vector normal to the contact surface during grasp, which can be obtained from the intrinsic tactile algorithm. The global ball center position estimate $\mathbf{b}$ can then be obtained as

$$\mathbf{b} = \frac{1}{n_f} \sum_{i=1}^{n_f} \mathbf{b}_i. \tag{3.6}$$

This can be used to distinguish the initial and final transient phases from the holding phase. Figures 3.7(a)-3.8(a) show plots of $\mathbf{b}$ for the two trials considered, each with the time frame of interest highlighted by two vertical dashed lines, while Figures 3.7(b)-3.8(b) show plots of the percentage error during such time frame. Tables 3.2 and 3.3 report numerical values of both absolute and percentage force Root Mean Square Error (RMSE) for both tasks. Torque error is also reported. It is worth noting that there is no intuitive choice of a normalization quantity for torques; for this reason only absolute torque error is shown.

3.7b and 3.8b show the behaviour of the error normalized during all the grasp.

| Components | $f_x$ | $f_y$ | $f_z$ |
|---|---|---|---|
| RMSE | 0.27 [N] | 0.30 [N] | 0.34 [N] |
| Percentage RMSE | 2.22 % | 2.66 % | 2.79 % |

| Components | $\tau_x$ [Nmm] | $\tau_y$ [Nmm] | $\tau_z$ [Nmm] |
|---|---|---|---|
| RMSE | 19.80 | 22.11 | 18.52 |

Table 3.2: Error for experiments with the ball of mass $m_1 = 0.053$ Kg.

| Components | $f_x$ | $f_y$ | $f_z$ |
|---|---|---|---|
| RMSE | 0.17 [N] | 0.29 [N] | 0.15 [N] |
| Percentage RMSE | 1.28 % | 2.17 % | 1.46 % |

| Components | $\tau_x$ [Nmm] | $\tau_y$ [Nmm] | $\tau_z$ [Nmm] |
|---|---|---|---|
| RMSE | 13.68 | 16.18 | 8.44 |

Table 3.3: Error for experiments with the ball of mass $m_2 = 0.32$ Kg.

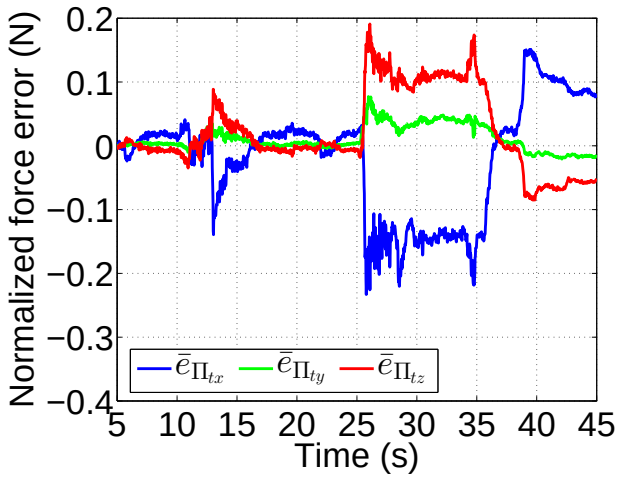


Figure 3.9: Internal force projection error components for the task with $n_f = 5$.

### 3.3.2 Experiments 2

In this experiment I exploit the force variation during the task. Let us consider $\Delta\mathbf{t} = \mathbf{t}_k - \mathbf{t}_0$, where $\mathbf{t}_0$ is the generalized force measured for an initial sample $s_0$ and $\mathbf{t}_k$ is the force measured in a later sample $s_k$. Since the ball is held still, the external wrench $\mathbf{w}$ is not changing, and from $\mathbf{w} = G\mathbf{t}_0 = G\mathbf{t}_k \ \forall k$ follows that $\Delta\mathbf{t}$ lies in the nullspace of $G$ ($\Delta\mathbf{t} \in \mathcal{N}(G)$). It is known from grasp theory and linear algebra ( [86], [87]) that $(I - G^+G)$ is a projector to $\mathcal{N}(G)$. Therefore, if we compute

$$\Pi_G(\Delta\mathbf{t}) := (I - G^+G)\Delta\mathbf{t} \tag{3.7}$$

since $\Delta\mathbf{t} \in \mathcal{N}(G)$ it should be true that $\Pi_G(\Delta\mathbf{t}) = \Delta\mathbf{t}$. The error $\mathbf{e}_\Pi \in \mathbb{R}^{30}$ can be defined as:

$$\mathbf{e}_\Pi := \Pi_G(\Delta\mathbf{t}) - \Delta\mathbf{t} \tag{3.8}$$

and the normalized error is defined consequently as:

$$\bar{\mathbf{e}}_{\Pi} := \frac{\mathbf{e}_{\Pi}}{\mathbf{E}_{\Pi}} \tag{3.9}$$

where $\mathbf{E}_{\Pi} \in \mathbb{R}^{30}$ is a vector that collect the maximum absolute values for each component of $\mathbf{e}_{\Pi}$. As an example, figure 3.9 shows the force components of normalized error of thumb $(\bar{\mathbf{e}}_{\Pi_{tx}}, \bar{\mathbf{e}}_{\Pi_{ty}}, \bar{\mathbf{e}}_{\Pi_{tz}})$ for the trial with the ball of mass $m_1$. A more complete representation of results can be found in Table 3.4, which shows RMSE considering only force components for the sake of space. RMSE for torques were all of the order of $10^{-3}$ N mm.

| Components | Thumb | Index | Middle | Ring | Little |
|---|---|---|---|---|---|
| $m_1 = 0.053$ Kg | | | | | |
| $f_x$ [N] | 0.077 | 0.10 | 0.085 | 0.082 | 0.073 |
| $f_y$ [N] | 0.036 | 0.72 | 0.17 | 0.034 | 0.10 |
| $f_z$ [N] | 0.075 | 0.068 | 0.14 | 0.15 | 0.32 |
| $m_2 = 0.32$ Kg | | | | | |
| $f_x$ [N] | 0.143 | 0.41 | 0.34 | 0.14 | n/a |
| $f_y$ [N] | 0.164 | 0.074 | 0.20 | 0.026 | n/a |
| $f_z$ [N] | 0.0063 | 0.054 | 0.030 | 0.13 | n/a |

Table 3.4: RMSE for the force components of $\mathbf{e}_{\Pi}$.

In this section I demonstrated the effectiveness of ThimbleSense to provide measurements of forces applied during grasping as well as to estimate the position of the contact point. The algorithm to deal the bias of F/T sensor allows to correct the contact forces in a correct manner. The Experimental validation to evaluate the accuracy

of measurements on grasps of two different balls, leads in both cases to force RMSE inferior to 0.35 N (less than 3% of the thumb force) and torque RMSE inferior to 23 Nmm. All these aspects make ThimbleSense a complementary tools of tripod device to investigate in a reasonable manner human grasp proprieties.

## 3.4 Conclusion

In this chapter I demonstrated the effectiveness of ThimbleSense to provide measurements of forces applied during grasping as well as to estimate the position of the contact point. The algorithm to deal the bias of F/T sensor allows to correct the contact forces in a correct manner. The Experimental validation to evaluate the accuracy of measurements on grasps of two different balls, leads in both cases to force RMSE inferior to 0.35 N (less than 3% of the thumb force) and torque RMSE inferior to 23 Nmm. All these aspects make ThimbleSense a complementary tools of tripod device to investigate in a reasonable manner human grasp proprieties. To investigate the force distribution in grasping tasks of robotic hand, solutions in order to adapt "ThimbleSense" on artificial manipulator will be considered.

# Part II

# Studies and Experiments on Three Digit Grasp

In the previous part a new set of devices to study the human grasp proprieties is described. More specifically the effectiveness of these systems in grasp analysis was also experimentally demonstrated and applications to neuroscientific studies are discussed. In the second part the tripod devices are exploited to investigate the principles performed by human to control the finger stiffness and the contact forces in tripod grasp tasks. To measures the stiffness at fingertip in a tripod grasp pose, in Chapter 4 a new technique is dealt; the identified stiffness patterns are then correlated with a EMG signals of dominant antagonistic pair of finger muscles in a suitable map. Chapter 5 presents a study on the correlation between the stiffness of the grasped object and the co-contraction activity of the dominant antagonistic pair of finger muscles.

Chapter 4

# Electromyographic Mapping of Finger Stiffness in Tripod Grasp

In the first part I described and validated a tripod device with easy to change contact surfaces of customizable stiffness; in this chapter I profitably integrate this device in a new set-up to identify the stiffness of hand finger tips in a tripod grasp pose. The stiffness pattern are after correlated with the EMG signals of flexor/extensor muscles of fingers to identify a possible map. Understanding the policy used by human to modulate the stiffness in grasping task, is important to develop suitable control in robotics, rehabilitation and tele-operation. As previously said in Chapter 1 few studies investigate about finger stiffness control performed by human in grasping tasks.

In [88] the authors evidence the ability of hand motor control to modulate the antagonist co-contraction activity for different tasks: monitoring limb position, decelerating the limb in ballistic movements and increasing stiffness [88]. Stiffening behaviour can be realized to stabilize movement or to fix posture in isometric tasks [28]. Previous work examining finger and hand stiffness has explored various topics including the mechanical impedance of the fingers [29] or at the fingertip [30], pinch grasp stiffness during an isometric grasp task [31],

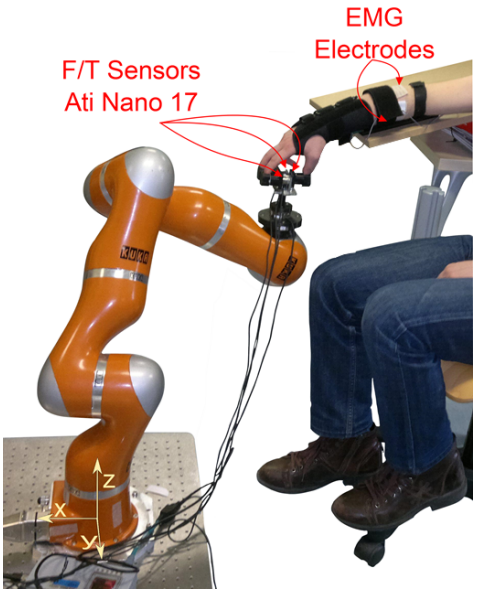


Figure 4.1: Experimental setup used for the trials. The KUKA applies planar perturbations to the fingers of the subject and the resulting forces are measured at the fingertips along with the surface EMG signals from the FDS and EDC muscles.

or variance of stiffness depending on finger force or posture [32]. The estimation of the impedance parameters in these studies is mainly achieved by an off-line post-processing phase, imposing severe limitations in real-time applications such as tele-impedance control of the prosthetic or robotic hands which require that the motion and the stiffness profiles of the fingers are appropriately commanded. At first, this might imply that an individual modelling and control of the finer motion and stiffness trajectories are required to perform a target manipulation task. However, observations in human motor control suggest that central nervous system solves for this complexity in an elegant and coordinated manner which has been well-recognized with the concept of hand synergies [89–91]. While the exploitation of this concept in kinematic coordinates has lead to the development

of several simple, effective and adaptive robotic designs and control strategies (e.g. see [13, 91]), its extension to dynamic coordinates, such as coordinated stiffening of the hand fingers, remains to be investigated.

Toward the twofold purpose of investigating the presence of coordinated regulations of the finger stiffness in human hand and the establishment of a real-time technique in modelling and identification of the finger stiffness while grasping, this study [A4] explores the relation between the fingertip stiffness and the EMG activity of the antagonist muscles contributing to this profile. To achieve this, the experiments are performed with a custom version of tripod-grasp device presented in Chapter 2. While constrained in a tripod posture subjects held a stable level of stiffness and experienced a series of perturbations provided by the KUKA lightweight robot arm. EMG was recorded alongside force/torque measurements. Consequently, the map between the fingertip stiffness profiles, is calculated from the force/torque measurements, and the EMG data.

## 4.1 Study Design

Five subjects participated in the experiment, 3 males and 2 females aged $28 \pm 3$ years. Before participating, subjects gave their informed consent. Subjects placed their fingers in a Tripod Device and maintained a steady level of hand stiffness, as measured by surface EMG, while experiencing perturbations provided by the KUKA lightweight robot (Figure 4.1). Subjects completed the first trial while relaxed and then increased stiffness to low, medium, and finally high levels in subsequent trials. The block of four trials was repeated three times for a total of 12 trials. Each perturbation trial lasted 35 seconds and the experiment lasted less than an hour.

### 4.1.1 Tripod Device and Experimental Setup

The Tripod Device is a custom version of the instrumented manipulandum presented in Section 2.2, this device can be grasped with three fingers and includes three individual contact surfaces. Each contact surface consists of a contact module rigidly attached to the structure of the manipulandum, through an interface engineered in Acrilonitrile-Butadiene-Stirene (ABS) rapid prototyping material. Each contact module consists of a cylindrical base in ABS (rigid case, Young Modulus 1.4 GPa). The structure of the manipulandum was fabricated in aluminium using a CNC (Computer Numerical Control) machine to ensure structural rigidity.

A force-torque sensor (Series Nano 17 by ATI, Apex, NC, USA) was positioned below the interface where each contact module was attached to measure the force and torque components applied by each finger. A finger-slot was designed and fixed to each contact surface to minimize the relative movements between the finger and the Tripod Device. A fourth F/T sensor (Series Nano 45 by ATI, Apex, NC, USA) placed at the base of the structure provided an independent measure of the external wrench. An exploded drawing view of the manipulandum with dimensions is reported in Fig. 5.2.

The Tripod Device was mounted at the end-effector of a 7-DOF robot arm: the KUKA lightweight robot (KUKA/DLR). All force and displacement measures were reported in the base reference frame of the KUKA. The KUKA, which has a positioning repeatability of $\pm 5$ mm, was programmed to follow a planar random trajectory, keeping the orientation angles of the end-effector (roll, pitch, yaw) constant, so that the Tripod Device remained parallel to the ground maintaining the same orientation with respect to the fixed frame. The subjects adopted a tripod posture and inserted the index finger, the middle finger, and the thumb in the dedicated finger-slots of the Tripod Device. At each finger, the forces in response to the position perturbation were measured by the contact point F/T sensors described above. Surface EMG signals on the forearm were measured and amplified with a

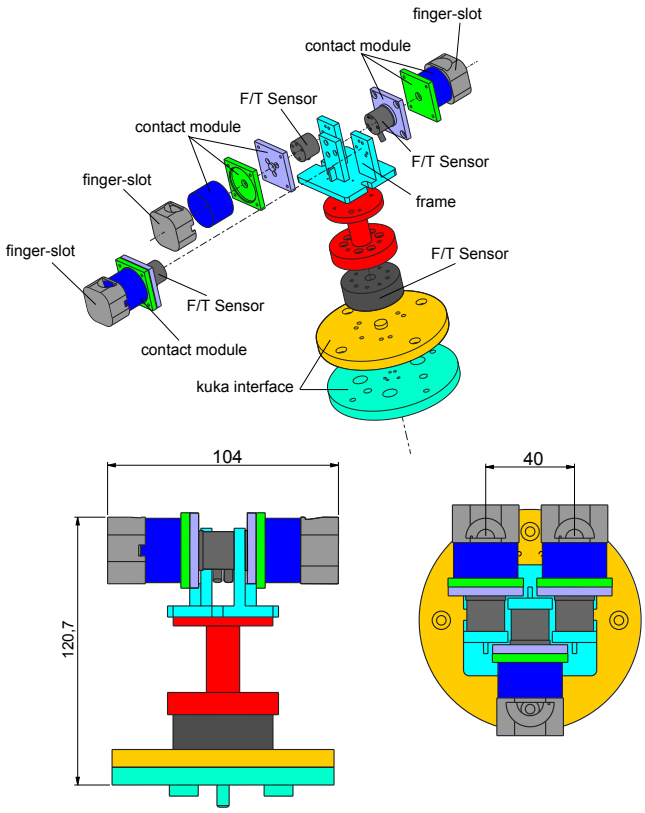


Figure 4.2: Exploded drawing view of the Tripod Device and its main features with dimensions in [mm].

Delsys-Bagnoli 16 (Delsys Inc.). The data acquisition and synchronization interface between the KUKA controller, the four F/T sensors, and the EMG acquisition board were developed in Microsoft Visual C++ environment.

### 4.1.2 Protocol

Subjects were seated for the duration of the experiment. Surface EMG electrodes were placed on the flexor digitorum superficialis (FDS) and

extensor digitorum comunis (EDC) muscles. To minimize cross-talk from neighboring muscles, the electrodes were positioned following the methods described by Perrotto et al. [92]. The subject's arm was immobilized against a board at an angle to allow the tripod grasp to be comfortably maintained parallel to the ground, see Fig. 4.1. In a pre-trial, the KUKA did not perturb the subject, and the subject was instructed to produce maximum hand stiffness without squeezing the tripod object. The level of co-contraction produced in this trial was used as an upper-bound for the stiffness level in subsequent trials. In the first trial, the subject placed his thumb, index, and middle fingertips in the finger-slots of the Tripod Device and remained relaxed while the KUKA perturbed the subject following the trajectory described above. In subsequent trials, subjects were asked to produce roughly 20, 40, or 60% of their maximum stiffness while the KUKA perturbed the hand; subjects were provided visual feedback to aid maintaining these levels. Subjects were also instructed to prioritize stability of stiffness level over accuracy of targeted level; that is, subjects aimed to keep a low standard deviation over producing a particular mean stiffness level. The block of four trials was repeated three times for a total of 12 trials.

## 4.2 Data Analysis

To estimate the endpoint stiffness at each of the three fingers, I adopted the same techniques used in [62] for the arm. Following Perrault et al. [93], a continuous stochastic perturbations is applied for 35 seconds to the subject's fingers through the Tripod Device. The perturbations were applied in x and y directions, with a peak-to-peak value of 10 mm in each direction and with a frequency spectrum that was flat in the range of 0 to 6Hz and null elsewhere. The first 5 seconds of data were discarded to allow the subject to reach the required stiffness level.

For each finger, the multiple-input, multiple-output (MIMO) dy-

namics of the endpoint stiffness were decomposed into four linear single-input, single output (SISO) subsystems; the identification of each SISO subsystem was performed in the frequency domain using a nonparametric algorithm [94]. The endpoint inertia, viscosity and stiffness matrices, $I$, $B$ and $K$, where found by comparing each SISO transfer function with a second order linear model of the type:

$$G_{i,j}(s) = I_{i,j}s + B_{i,j}s + K_{i,j}s, \quad i,j = x,y.$$

The external wrench measured at the base of the Tripod Device with the ATI Series Nano 45 force/torque sensor was compared with the external wrench derived from the three force-torque sensors placed under the fingers to verify that the measurements were correct. The surface EMG signals were acquired with a Delsys-Bagnoli 16 apparatus, sampled at 750Hz, high-pass filtered at a cut-off frequency of 4 Hz with a 4th order Butterworth filter. The resulting rectified signal was low-pass filtered in order to obtain its envelope. The average values of the EMG signals relative to the FDS and EDC muscles, respectively $p'$ and $p''$, were calculated at each trial. The resulting level of co-contraction $Lcc$ was computed as:

$$Lcc_{s,t} = \frac{1}{2}\left(\frac{p'_{s,t}}{p'_{s,\max}} + \frac{p''_{s,t}}{p''_{s,\max}}\right)$$

Where $s$ indicates the subject, $t$ the trial number and $p'_{s,\max}$, $p''_{s,\max}$ the maximum EMG values recorded respectively at channel 1 and channel 2 of subject $s$.

## 4.3 Results

Figure 4.3 shows the x component of a typical endpoint displacement $d(t)$ along with the x component of the resulting force $F(t)$ measured at the index fingertip. To evaluate the linear dependency of each output (forces) to all system inputs (displacements), the multiple coherence indices were computed on the obtained measurements. A

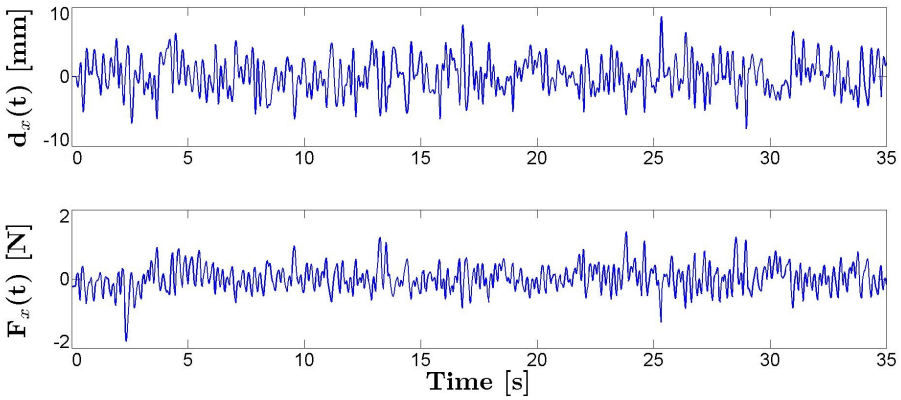


Figure 4.3: x components of a typical endpoint displacement $d(t)$ and the resulting force $F(t)$. $F(t)$ and $d(t)$ were used to estimate the endpoint stiffness of the fingers by means of a nonparametring algorithm in the frequency domain [94].

strong linear dependency of the inputs and the outputs was found in the frequency range 0-6 Hz, as shown in the Figure 4.4; for this reason the parameter estimation was performed in the same range.

After estimating each stiffness matrix $K$, its symmetric $K_s$ and asymmetric $K_a$ parts were extracted:

$$K_s = \frac{1}{2}(K + K^T) \qquad K_a = \frac{1}{2}(K - K^T)$$

The error of approximation was computed as:

$$e = \frac{||Ka||_2}{||Ks||_2},$$

obtaining a mean value $\bar{e} \approx 0.07$.

The eigenvalues $\lambda_1$ and $\lambda_2$ (with $\lambda_1 < \lambda_2$) of Ks and the corresponding eigenvectors, $\mathbf{v_1}$ and $\mathbf{v_2}$, were computed. In all of the

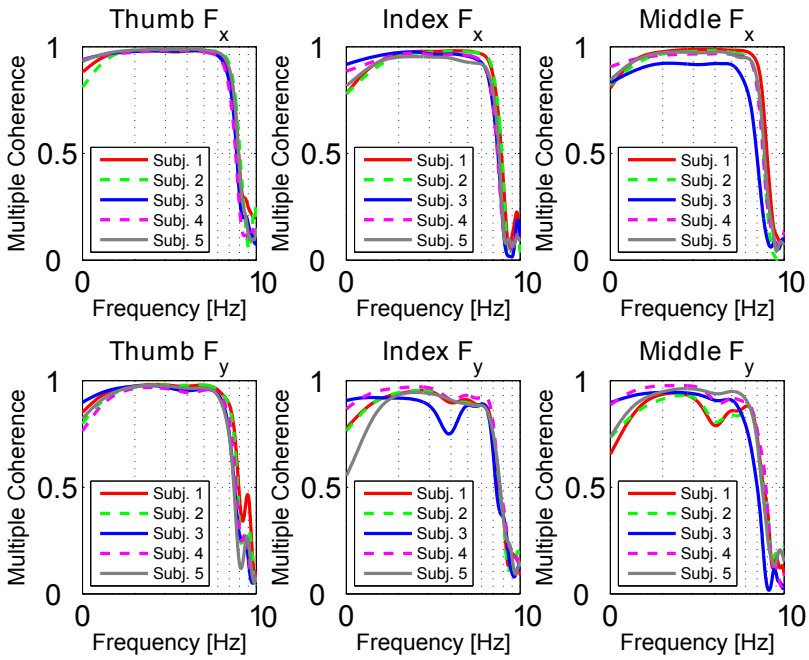


Figure 4.4: Example of Multiple Coherence function values for the five subjects.

examined cases, Ks was found to be positive definite, with $\lambda_1$ and $\lambda_2$ real and greater than 0.

Figure 4.5 presents the endpoint stiffness ellipses that were generated by one of the subjects during four consecutive trials (with four different indications on the stiffness set-point level). Stiffness ellipses are a consolidated method of representing the endpoint stiffness. In the 2D case, the major and minor axes of the ellipse represent respectively $\lambda_2$ and $\lambda_1$, while the orientation $\theta$ of the ellipse is given by the angle between $\mathbf{v_2}$ and the x axis. As expected, the stiffness ellipse area ($A = \pi\lambda_1\lambda_2$) increases with increasing targeted stiffness levels. On the other hand, the orientation $\theta$, as well as the shape (here quantified with the ratio $\frac{\lambda_1}{\lambda_2}$), of the stiffness ellipse does not appear

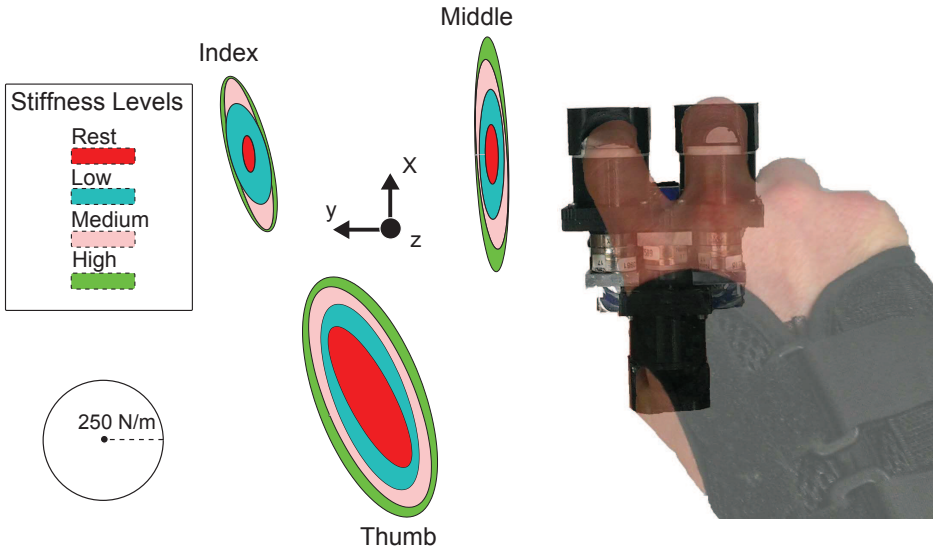


Figure 4.5: Endpoint stiffness ellipses generated by one of the subjects during four consecutive trials.

to be correlated with the stiffness levels. Table 4.1 reports the mean values of the of the stiffness ellipses' orientations corresponding to different stiffness levels. For each subject, the values are distributed in three different rows $I$, $M$ and $T$ that correspond respectively to the index finger, middle finger and thumb. Following the same structure of Table 4.1, Table 4.2 presents the average ratio $\frac{\lambda_1}{\lambda_2}$ with respect to different stiffness levels.

To further investigate the behavior of the stiffness components $\lambda_1$ and $\lambda_2$ at each finger, I used the measured surface EMG signals from the FDS (channel 1) and EDC (channel 2) muscles as an indicator of the global stiffness of the hand. Figure 4.6 shows the filtered EMG signals acquired from one of the subjects during three different trials. The three trials corresponded to three increasing levels of stiffness.

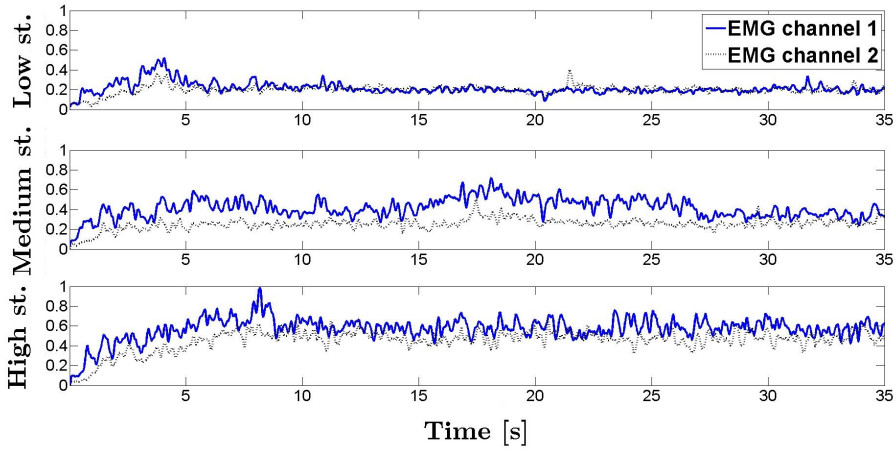


Figure 4.6: Typical normalized EMG signals for three different levels of stiffness.

Each signal was normalized to the maximum value produced by the subject during the pre-trial phase for the corresponding EMG channel.

The acquired EMG signals were used to compute the *Lcc* index for each trial. To measure the correlation between the stiffness components at each finger and the *Lcc* index, Pearson's Correlation Coefficient (PCC) was used. PCC produces a measure of the linear correlation between two measures; it can range from $-1$ (total negative correlation) to 1 (total positive correlation), with 0 indicating absence of correlation. The average correlation coefficient obtained between $\lambda$ and *Lcc* was:

$$\overline{PCC} \approx 0.81$$

For each subject the norm values of $\lambda_1$ and $\lambda_2$ are fitted with respect to *Lcc*. A total of six fittings were performed for each subject (two per finger) by implementing least-squares regression to find the

Table 4.1: Average ellipse orientations for the four levels of stiffness.

| $\theta(^\circ)$ | **Finger** | **Rest** | **Low St.** | **Medium St.** | **High St.** |
|---|---|---|---|---|---|
| Subject 1 | $I$ | 8.1 | 10.3 | 0.2 | 5.7 |
| | $M$ | 12.1 | 14.6 | 15.5 | 15.6 |
| | $T$ | 10.6 | 14.0 | 14.2 | 19.1 |
| Subject 2 | $I$ | 20.8 | 22.4 | 24.1 | −15.0 |
| | $M$ | 24.8 | 25.9 | 32.2 | 22.8 |
| | $T$ | 12.3 | 1.5 | −6.1 | 0.5 |
| Subject 3 | $I$ | −1.6 | 3.1 | 4.1 | 4.1 |
| | $M$ | 28.2 | 7.5 | 2.3 | 3.2 |
| | $T$ | 5.4 | 11.4 | 2.5 | −2.0 |
| Subject 4 | $I$ | 34.1 | 8.9 | 6.7 | −11.6 |
| | $M$ | 27.3 | 15.6 | 20.5 | 24.7 |
| | $T$ | 27.3 | 23.5 | 22.0 | 22.9 |
| Subject 5 | $I$ | 15.3 | 13.5 | 15.5 | 16.7 |
| | $M$ | 15.2 | 18.1 | −10.7 | −25.7 |
| | $T$ | 13.7 | 20.3 | 23.3 | −10.2 |

coefficients $m_{i,f}$ and $q_{i,f}$ in the following equation:

$$\frac{\lambda_{i,f}}{\lambda_{i,f}^{\text{MAX}}} \approx m_{i,f} Lcc + q_{i,f} \qquad i = 1, 2$$

Table 4.2: Average ratio $\frac{\lambda_1}{\lambda_2}$ of the ellipse axes for the four levels of stiffness.

| $\frac{\lambda_1}{\lambda_2}$ | **Finger** | **Rest** | **Low St.** | **Medium St.** | **High St.** |
|---|---|---|---|---|---|
| Subject 1 | $I_1$ | 0.13 | 0.09 | 0.19 | 0.25 |
| | $M_1$ | 0.27 | 0.31 | 0.27 | 0.23 |
| | $T_1$ | 0.19 | 0.14 | 0.16 | 0.17 |
| Subject 2 | $I_2$ | 0.41 | 0.34 | 0.31 | 0.30 |
| | $M_2$ | 0.37 | 0.26 | 0.22 | 0.19 |
| | $T_2$ | 0.22 | 0.17 | 0.20 | 0.30 |
| Subject 3 | $I_3$ | 0.22 | 0.19 | 0.17 | 0.16 |
| | $M_3$ | 0.51 | 0.29 | 0.26 | 0.32 |
| | $T_3$ | 0.48 | 0.44 | 0.32 | 0.20 |
| Subject 4 | $I_4$ | 0.61 | 0.43 | 0.61 | 0.58 |
| | $M_4$ | 0.07 | 0.32 | 0.42 | 0.40 |
| | $T_4$ | 0.23 | 0.31 | 0.40 | 0.46 |
| Subject 5 | $I_5$ | 0.14 | 0.14 | 0.18 | 0.21 |
| | $M_5$ | 0.18 | 0.25 | 0.33 | 0.19 |
| | $T_5$ | 0.17 | 0.23 | 0.26 | 0.40 |

Table 4.3: Angular coefficients $m_{i,f}$ of the fitting lines along with the average coefficient of determination $R^2$ for each subject.

| | $m_{1,I}$ | $m_{2,I}$ | $m_{1,M}$ | $m_{2,M}$ | $m_{1,T}$ | $m_{2,T}$ | $R^2$ |
|---|---|---|---|---|---|---|---|
| $Subject1$ | 1.20 | 1.25 | 1.13 | 1.17 | 1.25 | 0.71 | 0.73 |
| $Subject2$ | 1.19 | 1.18 | 0.93 | 0.96 | 1.11 | 0.61 | 0.86 |
| $Subject3$ | 1.31 | 1.33 | 1.14 | 1.34 | 0.91 | 0.53 | 0.72 |
| $Subject4$ | 0.88 | 0.74 | 0.45 | 0.67 | 0.70 | 0.50 | 0.42 |
| $Subject5$ | 1.68 | 2.60 | 2.13 | 1.67 | 1.95 | 1.13 | 0.60 |

where $f = T, I, M$ indicates thumb, index or middle finger, respectively, and $\lambda_{i,f}^{\text{MAX}}$ is the maximum value of $\lambda_{i,f}$ among the 12 trials. The results for one of the subjects are presented in Figure 4.7. The slopes of the fitting lines for each subject along with the mean coefficient of determination $R^2$ are given in table 4.3.

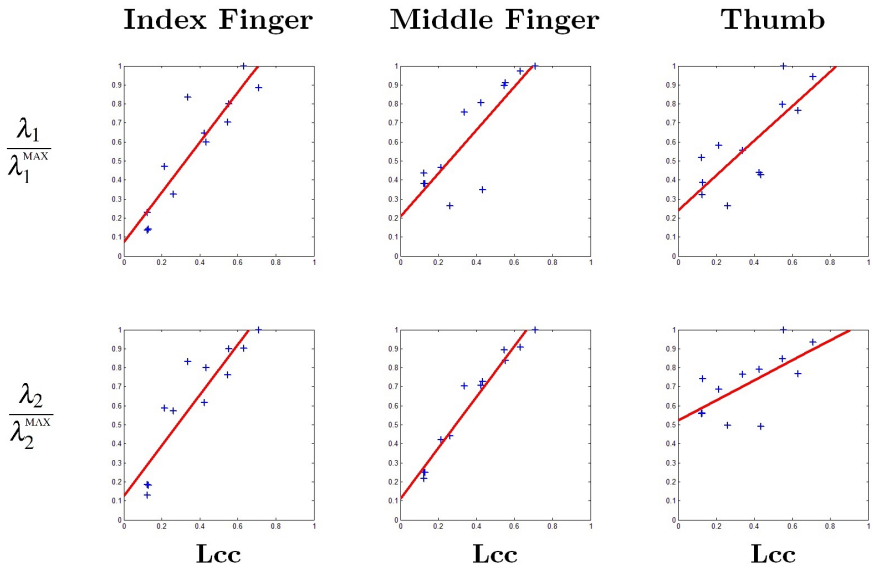


Figure 4.7: Linear regression of normalized stiffness axes with respect to the level of co-contraction *Lcc*. The graphs are relative to Subject 3.

## 4.4 Discussion

The experimental results corroborate the feasibility of a generalized mapping between the EMGs recorded from the FDS and EDC muscles and the hand stiffness. Since the aim of this work was not the generation of an accurate model of hand stiffness control but instead to move a step towards the design of more natural and better performing control interfaces for hand prostheses and teleoperation, I focused only on the relationship between the hand stiffness and the FDS and EDC muscles. In particular, I represented the endpoint stiffness of the fingers with stiffness ellipses and found that their area increased with respect to increasing levels of co-contraction *Lcc*, while their orientation and shape did not seem to be related to *Lcc*. In fact, the variation of $\theta$ and $\frac{\lambda_1}{\lambda_2}$ across trials as seen in Table 4.1 and 4.2 does

not appear to depend on the stiffness level; this conjecture is supported by the studies on the human limb stiffness, which state that the orientation and shape of the endpoint stiffness ellipses is mainly determined by posture [95]. In general, the endpoint stiffness of the thumb, index and middle fingers was found to increase when the level of co-contraction *Lcc* increased. Furthermore, the results of the linear fittings (Table 4.3) show that, not only the relationship between stiffness and *Lcc* was nearly linear, but also that, with the exception of $m_{2,T}$, the slopes of the fitting lines tend to maintain a similar value among the same subject. This result is very important because it highlights a tendency of the fingers to stiffen in a coordinated way that is also proportional to the level of co-contraction of the EDC and FDS muscles. However, in order to produce a simple but efficient generalized mapping between hand stiffness and co-contraction, further studies should be conducted. In particular, this work is focused on the relationship between co-contraction and hand stiffness in absence of grip force. The subjects were in fact asked not to produce any grip force and, by checking the force/torque measurements, it's found that the request was fulfilled in all the trials with the exception of Subject 4 and Subject 5 during the high stiffness condition. This simplification was made in order to better understand the role of co-contraction in the control of hand stiffness, but it will also take into account the possibility of the exertion of grip forces to profitably use the mapping in real tasks.

## 4.5 Conclusion

In this section, a reasonable approach to characterize and map the hand stiffness is presented. To the best of my knowledge, this is the first work that analyses the relationship between co-contraction of the FDS and EDC muscles and the endpoint stiffness of thumb, index and middle finger; the results suggest that, while the shape and orientation of the stiffness ellipses are mainly influenced by the hand posture,

there is a nearly linear relation between the level of co-contraction and the length of the ellipses' axes. Furthermore, by normalizing the endpoint stiffness components of each finger, it's possible to identify a rate of growth between the stiffness components and the level of co-contraction that had little variations among different fingers of the same subject. These results show the feasibility of a generalized mapping between the EMGs recorded from the FDS and EDC muscles and the hand stiffness. Such a mapping could be applied to many disciplines of robotics, in particular it could allow the design of more natural and efficient control schemes for upper limb prostheses.

Chapter 5

# Effect of Homogenous Object Stiffness on Tri-digit Proprieties

## 5.1 Introduction

In the previous chapter I evidenced a relation between finger stiffness and EMG signals of principal finger muscles; in this study I monitored the same muscle activity throughout the grasp of a tripod device with different stiffness at contact points. To investigate the effect of the stiffness at contact point on the grasping force distribution, I profitably used the tools and method presented in the previous chapters. In effect grasping of compliant objects presents additional uncertainties and Winges et al. [18] showed that, during a grasp, when one or two contact points are compliant, the activation patterns of finger muscles are different with respect to the case where the contact points are rigid. Besides analyzing the grip forces, to fully understand the control of hand grasping by the CNS, it is important to study how the hand stiffness is regulated during a grasp: stiffening behavior is commonly realized to stabilize movement or to fix posture in isometric tasks [28] and recent findings suggest that, to some extent, grip stiffness is independent from grip force [70].

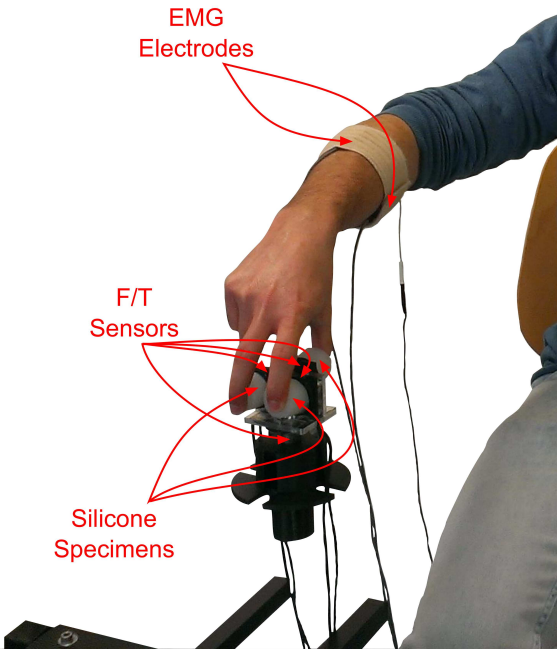


Figure 5.1: Experimental setup used for the trials.

This study [A5] aims to investigate the relation between object compliance and grasping stiffness of the hand. To achieve this goal, 11 subjects perform a grasp experiment exploiting a modified version of the Tripod Device (see Section 2.2) with three different contact modules. Each module is characterized by a certain level of stiffness: rigid, high, medium, or low stiffness. The experiment consisted of four blocks of trials, corresponding to the four different levels of stiffness; in each trial the subject grasped and lifted the Tripod Device 25 times while the EMG was recorded from the Flexor Digitorum Superficialis (FDS) and Extensor Digitorum Comunis (EDC). These two muscles are the main finger antagonist pair and thus can be used to monitor the EMG activity resulting in the production of grasp force as well as overall hand stiffness; this assumption is in agreement with the capability of the human control system to increase hand stiffness

exploiting the co-contraction of antagonist muscles ( [88]).

## 5.2 Materials and Methods

### 5.2.1 Study Design

Eleven healthy volunteers participated in this study (5 males and 6 females, mean age 28 ± 3 years, 10 right-handed). Before starting the study, all participants signed an informed consent previously approved by the regional ethics committee. The study consisted of four blocks of 25 trials each in which the subject grasped and lifted the Tripod Device while EMG was recorded from the main finger flexor and extensor muscles. The device was held steady for a brief period and placed back on a table. At the contact points for the thumb, index, and middle fingers, an interface of varying rigidity was placed. Three silicone interfaces of compliant, medium, and high stiffness were used as well as a rigid ABS plastic interface covered in a thin film of silicone, to match haptic conditions. The order of the four block conditions was randomized to reduce order effects.

### 5.2.2 Tripod Device and Experimental Setup

The Tripod Device is a custom version of instrumented manipulandum developed to study three-finger grasps in Section 2.2. Several sets of contact modules were designed to include contact surfaces with different levels of stiffness. Each contact module include an interface engineered in Acrilonitrile-Butadiene-Stirene (ABS) rapid prototyping material to allow them to be rapidly interchanged on the device. The manipulandum is equipped with an internal frame made in aluminium using a CNC (Computer Numerical Control) machine to ensure structural rigidity. A set of cylindrical interfaces in ABS or silicone were integrated with the contact module, each with a different level of stiffness. The silicone was obtained by mixing a given quantity of a commercial bicomponent, room temperature-curing silicone

(BJB TC-5005A/B), with different percentage of plasticizer (BJB TC-5005C), acting as a softener. Softener was mixed at a percentage of 45%, 20%, 0% as shown in [79] to obtain three different stiffness levels. A fourth specimen was made only with ABS. The four different contact surfaces have a Young's Modulus of 200 kPa, 500 kPa, 750 kPa and 1.4 GPa and are referred to as low-, medium-, and high-stiffness silicone and rigid ABS conditions, respectively.

The force and torque components applied by each finger are measured by three force-torque sensors (Series Nano 17 by ATI, Apex, NC, USA) fixed below each contact module. The effect of cables and the external wrench are monitored by a fourth F/T sensor (Series Nano 17 by ATI, Apex, NC, USA) placed at the base of the structure. An exploded drawing view of the manipulandum with dimensions can be found in Fig. 5.2. The total weight of the manipulandum, including the sensor cables was 300 g. The Tripod Device was built to allow an additional component to be attached at the base to easily change the weight of the device; in this experiment, an additional 100g was used for a total device weight of 400g. Surface EMG signals on the forearm were measured and amplified with a Delsys-Bagnoli 16 channel system (Delsys Inc.). The data acquisition and synchronization were performed in Simulink (Matlab R2012a) software exploiting Data Acquisition Toolbox, Instrument Control Toolbox, and Simulink Block for Real Time Execution.

### 5.2.3 Protocol

Surface EMG sensors were placed on the main muscle belly of the flexor digitorum superficialis (FDS) and extensor digitorum communis (EDC) muscles following the identification and verification procedures outlined in [92]. Maximum voluntary contractions (MVC) were then collected for each muscle by asking subjects to contract against resistance provided by the experimenter. Subjects were seated in front of the tripod device, which was placed on a table. The device was equipped with the appropriate contact stiffness interface, according to

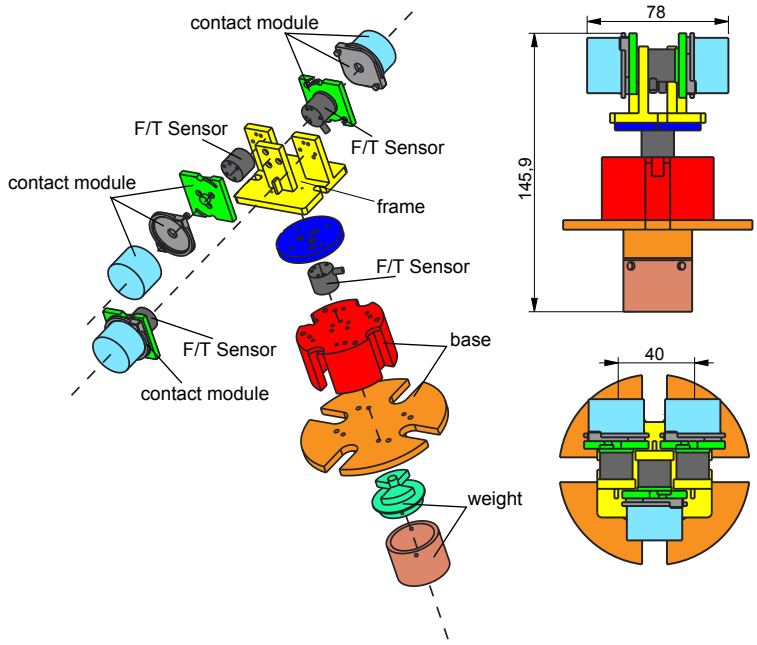


Figure 5.2: Exploded drawing view of the Tripod Device and its main features with dimensions in [mm]

the randomization table. Subjects were instructed to lift the object vertically, avoiding object tilt as much as possible. (Note: in order to encourage as natural a grasp as possible, subjects were given no instruction as to grasp force, eg: to use the minimum force necessary to lift the device.) After a brief (1-2 second) pause, sujects then placed the tripod device back on the table. This procedure was repeated for 25 total lifts. Subjects proceeded at their own pace and were allowed to pause as needed to avoid fatigue both during the block of 25 trials and between blocks. After each block, the interface was changed to a new stiffness condition and a new block of 25 trials conducted until subjects had completed all four conditions.

## 5.3 Data Analysis

The first five trials in each block were discarded to avoid learning or crossover effects. The vertical axis of the FT sensor at the base of the manipulandum was used to segment the data into lift, hold, and place phases of the subsequent 20 trials. The mean was subtracted from the EMG data to remove the DC offset before rectifying the data. EMG data was then normalized to the maximum contraction collected prior to the trials. The average value of the hold phase of the EMG and the normal force exerted by each finger was then calculated. The data were further synthesized into an average value for each condition for each subject. To perform group analysis, a repeated measures analysis of variance (RM ANOVA) was used. The RM ANOVA was performed on four sets of data: FDS and EDC EMG levels, cocontraction levels, and the sum of the index and middle finger contact point forces. When a main effect of stiffness was found, the data was then subjected to a post-hoc analysis using Bonferroni corrections for multiple comparisons.

## 5.4 Results

All subjects tolerated the protocol well, and each session lasted approximately an hour, including set-up and self-timed breaks. Subjects occasionally reported low levels of fatigue and were encouraged to break as needed to minimize fatigue effects. Measurements from a sample trial are shown in Fig. 5.7: the normal forces and the weight in Fig. 5.3 and 5.4; the values of the EMG signals in the same time range in Fig. 5.5 and 5.6. A summary of the FDS, EDC, and cocontraction EMG data can be found in Fig 5.8. The group data was analyzed using RM ANOVA, as detailed in the preceding section. The FDS data violated the assumption of sphericity (using Mauchly's test, $p \ll 0.01$), therefore the Greenhouse-Geisser correction was applied ($\epsilon = 0.446$). No effect of stiffness condition on FDS contraction levels was found ($F=3.592$, $p=0.071$). In contrast, there was a main

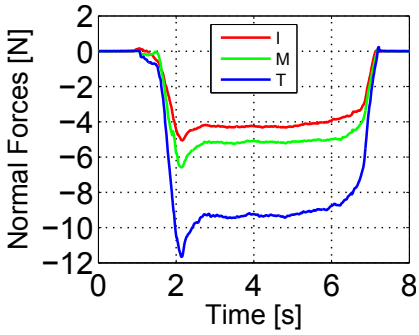


Figure 5.3: Normal forces exerted by thumb, index and middle fingers

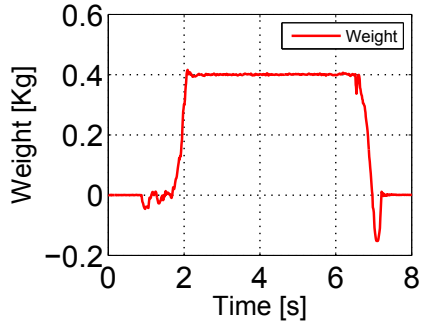


Figure 5.4: Weight of the object measured by the FT sensor

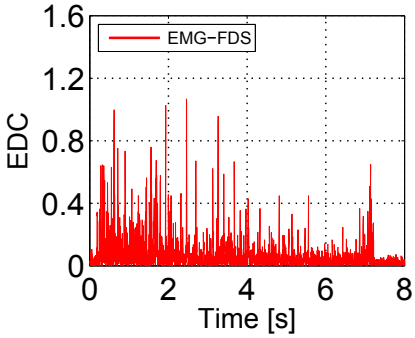


Figure 5.5: EMG signal of FDS muscle

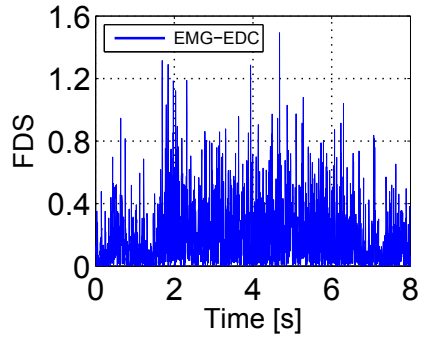


Figure 5.6: EMG signal of EDC muscle

Figure 5.7: An example of the measurements collected in one trial

effect of stiffness condition on EDC contraction ($F=9.942$, $p \ll 0.01$). This analysis was thus followed by post-hoc tests with Bonferroni corrections: EDC activity during the low-stiffness silicone condition was found to be significantly different from the high-stiffness silicone and rigid ABS conditions ($p=0.021$ and 0.001, respectively). Finally, the cocontraction values were analyzed: they violated Mauchly's test of sphericity ($p=0.006$), therefore the Greenhouse-Geisser correction

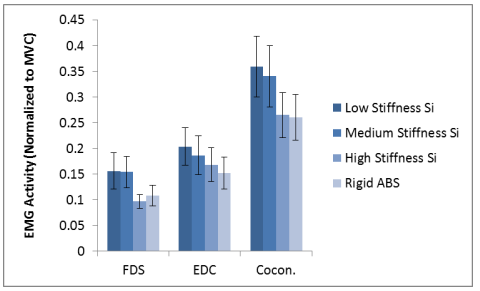


Figure 5.8: Average values of FDS, EDC, and cocontraction normalized to MVC, with standard error bars.

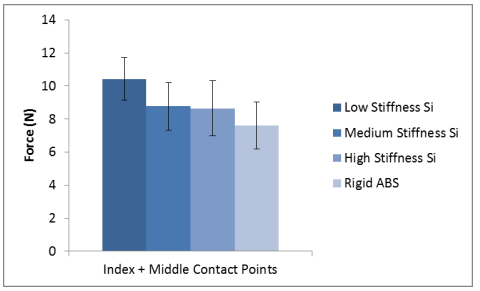


Figure 5.9: Average force at the index and middle finger contact points, normalized to MVC, with standard error bars.

was again applied ($\epsilon = 0.583$). There was a main effect of stiffness condition (F=6.280, p=0.011) and post-hoc tests showed a significant difference between rigid ABS conditions and low-stiffness as well as medium-stiffness silicone (p=0.045, 0.015, respectively).

To validate the sensor data, the normal force at the thumb contact point was subtracted from the sum at the index and middle finger contact points. The resulting difference was found to be near zero, as expected (data not shown). The average of the sum of the index and finger contact forces is plotted in Fig. 5.9. The index and middle finger contact force was analyzed using RM ANOVA as before and a main effect of condition was found (F=4.984, p=0.006). However, post-hoc analysis did not find any significant difference between con-

dition pairs, possibly due to the conservative nature of the Bonferroni correction.

## 5.5 Discussion and Conclusions

The study presented above examines the effect of the stiffness of an object on the EMG activity during a grasp and lift task. Eleven subjects participated in the experiment in which they grasped and lifted a tripod object with four different stiffness contact points. Although subjects generally seemed to exhibit higher FDS activity for more compliant conditions than more rigid conditions, results also showed large intra- and inter-subject variability. There was no significant difference due to stiffness conditions in the FDS activity. The EDC results, however showed a clearer trend of increasing activity with decreasing stiffness with a significant effect of stiffness. This trend was visible in the post-hoc results showing that grasping and lifting the low-stiffness silicone resulted in significantly higher EDC EMG activity than the two highest stiffness conditions. Finally, there was a main effect of stiffness on cocontraction levels, with post-hoc tests showing EMG cocontraction was significantly lower when grasping and lifting the rigid ABS compared to both the low- and medium-stiffness silicone. Together, these results suggest the co-contraction changes are primarily due to the increased EDC levels rather than a change in FDS levels.

To further undersand the meaning of the change in EMG levels, the contact forces are examined during each condition. Though there appears to be a trend toward increasing force with decreasing stiffness, and indeed a main effect of stiffness on force levels, post-hoc testing did not reveal any significant differences between specific condition pairs. It is possible that this effect is masked by the conservative nature of the Bonferroni correction. Taken in combination, these results suggest that the motor system responds to the increase in compliance by increasing the activity of the antagonist muscle, ultimately

resulting in higher cocontraction levels from the antagonist pair. The increased stiffness would thus serve to counterbalance the increased compliance, and thus instability, of the grasp.

The results shown here suggest a decoupling of flexor and extensor activity with changing object compliance, despite relatively stable grasp posture. As mentioned in the introduction, there is evidence that specific patterns of activation are used in grasp tasks; in the future, the effect of varying compliance without varying position on these patterns could be investigated. Further, it is worth noting that because the tripod object was grasped from above with only fingertip contact, subjects may have been more likely to increase stiffness to produce a more secure grasp, especially as the contact compliance increased. In a power or conformal grasp, this stiffness effect may thus be decreased due to the increased positional stability and thus reduced reliance on grasp force and/or stiffness. Future experiments will expand the results described above to examine the effects of contact stiffness on both power and precision grasps.

Chapter 6

# Conclusions

All the devices and the methods presented in this thesis are validated and usable for neuroscientific studies on human grasp force distribution and control. The two aforementioned approaches, "Sensorized Object " and "Wearable-Devices " allow to investigate the effect of different factors that could influence human grip control. These devices allow to collect all the necessary measurements to have a complete characterization of human grasp in terms of contact point locations, F/T measurements at contacts. Implementation of methods to deal offset of (F/T) sensors allow to ensure correctness of F/T measurements during grasp of the object without restriction on the object configurations.

In the second part of the thesis, the tripod device, was exploited in two studies to investigate human strategies to control the stiffness at contact points in grasping tasks.

In the first study, a reasonable approach to characterize and map the hand stiffness is presented. This is a pioneer work that analyses the relationship between co-contraction of the FDS and EDC muscles and the endpoint stiffness of thumb, index and middle finger; the results suggested that, while the shape and orientation of the stiffness ellipses are mainly influenced by the hand posture, there is a nearly

linear relation between the level of co-contraction and the length of the ellipses' axes. These results show the feasibility of a generalized mapping between the EMGs recorded from the FDS and EDC muscles and the hand stiffness.

The second study outcomes aim a decoupling of flexor and extensor activity with changing object compliance, despite relatively stable grasp posture. As mentioned in literature, there is evidence that specific patterns of activation are used in grasp tasks. These results suggest that humans prefer to increase the co-contraction of finger muscles when they grasp deformable objects. Resuming, the outcomes of this thesis are tangible contributions to: i) advance the state of art on human strategies in manipulation tasks and provide tools to assess rehabilitation procedures and ii) investigate human strategies for impedance control that can be used for human-robot interaction and control of myoeletric prosthesis. Future works could study the effect of object weight and cutaneous cues to evidence unknown strategies in human motor control. To study soft synergies model in human grasping tasks, the tools and methods presented in this thesis could be integrated with systems able to measure hand configurations during the grabbing phase.

To improve the performance of prosthetic/robotic hand in grasping task and to reduce the gap with human hand ability, the strategies evidenced in the second part of the thesis could be implemented in new class of control laws.

In rehabilitation scenarios the developed devices could be exploited: to evidence differences of grasp properties between healthy and disabled subjects and to assess the outcomes of rehabilitation therapies.

# Bibliography

## Author's

[A1] A. Altobelli, M. Bianchi, A. Serio, G. Baud-Bovy, M. Gabiccini, and A. Bicchi, "Three-digit grasp haptic device with variable contact stiffness for rehabilitation and human grasping studies," in *Mediterranean Conference on Control and Automation*, 2014, accepted.

[A2] A. Altobelli, M. Bianchi, M. Catalano, A. Serio, G. Baud-Bovy, and A. Bicchi, "An instrumented manipulandum for human grasping studies," in *ICORR*, 2015, accepted.

[A3] E. Battaglia, M. Bianchi, A. Altobelli, G.Grioli, M. Catalano, A.Serio, M.Santello, and A.Bicchi, "Thimblesense: a fingertip-wearable tactile sensor for grasp analysis," 2015, submitted.

[A4] M. Rossi, A. Altobelli, S. Godfrey, A. Ajoudani, and A. Bicchi, "Electromyographic mapping of finger stiffness in tripod grasp: a proof of concept," in *ICORR*, 2015, accepted.

[A5] S. Godfrey, A. Altobelli, M. Rossi, and A. Bicchi, "Effect of homogenous object stiffness on tri-digit grasp properties," in *EMBC*, 2015, accepted.

## Author's Videos

[B6] A. Altobelli, M. Bianchi, M. Catalano, A. Serio, G. Baud-Bovy, and A. Bicchi, "An instrumented manipulandum for human grasping studies," https://youtu.be/M7C2H-rZV70.

## Miscellaneous

[7] J. P. Kuhtz-Buschbeck, H. H. Ehrsson, and H. Forssberg, "Human brain activity in the control of fine static precision grip forces: an fmri study," *European Journal of Neuroscience*, vol. 14, no. 2, pp. 382–390, 2001.

[8] R. S. Johansson and J. R. Flanagan, "Coding and use of tactile signals from the fingertips in object manipulation tasks," *Nature Reviews Neuroscience*, vol. 10, no. 5, pp. 345–359, 2009.

[9] D. M. Wolpert, J. Diedrichsen, and J. R. Flanagan, "Principles of sensorimotor learning," *Nature Reviews Neuroscience*, vol. 12, no. 12, pp. 739–751, 2011.

[10] M. Santello, M. Flanders, and J. F. Soechting, "Postural hand synergies for tool use," *The Journal of Neuroscience*, vol. 18, no. 23, pp. 10 105 – 10 115, 1998.

[11] M. Gabiccini and A. Bicchi, "On the role of hand synergies in the optimal choice of grasping forces," in *Robotics Science and Systems*, 2010.

[12] A. Bicchi, M. Gabiccini, and M. Santello, "Modelling natural and artificial hands with sinergie," *Phil. Trans. R. Soc. B*, vol. 366, pp. 3153–3161, 2011.

[13] M. G. Catalano, G. Grioli, A. Serio, E. Farnioli, C. Piazza, and A. Bicchi, "Adaptive synergies for a humanoid robot hand," in *IEEE-RAS International Conference on Humanoid Robots*, Osaka, Japan, In Press.

[14] V. M. Zatsiorsky and M. L. Latash, "Multifinger prehension: an overview," *Journal of Motor Behavior*, vol. 40, no. 5, pp. 446–476, 2008.

[15] J. R. Flanagan, M. K. Burstedt, and R. S. Johansson, "Control of fingertip forces in multidigit manipulation," *Journal of Neurophysiology*, vol. 81, no. 4, pp. 1706–1717, 1999.

[16] G. Baud-Bovy and J. F. Soechting, "Two virtual fingers in the control of the tripod grasp," *Journal of Neurophysiology*, vol. 86, no. 2, pp. 604–615, 2001.

[17] ——, "Factors influencing variability in load forces in a tripod grasp," *Experimental brain research*, vol. 143, no. 1, pp. 57–66, 2002.

[18] S. A. Winges, S. E. Eonta, J. F. Soechting, and M. Flanders, "Effects of object compliance on three-digit grasping," *Journal of neurophysiology*, vol. 101, no. 5, pp. 2447–2458, 2009.

[19] M. Santello and J. F. Soechting, "Force synergies for multifingered grasping," *Experimental Brain Research*, vol. 133, no. 4, pp. 457–467, 2000.

[20] W. Zhang, A. M. Gordon, Q. Fu, and M. Santello, "Manipulation after object rotation reveals independent sensorimotor memory representations of digit positions and forces," *Journal of neurophysiology*, vol. 103, no. 6, pp. 2953–2964, 2010.

[21] Q. Fu, Z. Hasan, and M. Santello, "Transfer of learned manipulation following changes in degrees of freedom," *The Journal of Neuroscience*, vol. 31, no. 38, pp. 13 576–13 584, 2011.

[22] L. Dipietro, A. M. Sabatini, and P. Dario, "A survey of glove-based systems and their applications," *Systems, Man, and Cybernetics, Part C: Applications and Reviews, IEEE Transactions on*, vol. 38, no. 4, pp. 461 –482, 2008.

[23] T. R. Grieve, J. M. Hollerbach, and S. A. Mascaro, "Force prediction by fingernail imaging using active appearance models," in *World Haptics Conference (WHC), 2013*. IEEE, 2013, pp. 181–186.

[24] P. S. Lum, C. G. Burgar, P. C. Shor, M. Majmundar, and M. V. der Loos, "Robot-assisted movement training compared with conventional therapy techniques for the rehabilitation of upper-limb motor function after stroke," *Archives of Physical Medicine and Rehabilitation*, vol. 83, no. 7, pp. 952 – 959, 2002.

[25] H. I. Krebs, B. Volpe, M. Ferraro, S. Fasoli, J. Palazzolo, B. Rohrer, L. Edelstein, and N. Hogan, "Robot-aided neurorehabilitation: From evidence-based to science-based rehabilitation," *Topics in Stroke Rehabilitation*, vol. 8, no. 4, pp. 54–70, 2002.

[26] F. Carpi, G. Frediani, C. Gerboni, J. Gemignani, and D. De Rossi, "Enabling variable-stiffness hand rehabilitation orthoses with dielectric elastomer transducers," *Medical engineering & physics*, vol. 36, no. 2, pp. 205–211, 2014.

[27] J.-C. Metzger, O. Lambercy, and R. Gassert, "High-fidelity rendering of virtual objects with the rehapticknob-novel avenues in robot-assisted rehabilitation of hand function," in *Haptics Symposium (HAPTICS), 2012 IEEE*. IEEE, 2012, pp. 51–56.

[28] D. R. Humphrey and D. J. Reed, "Separate cortical systems for control of joint movement and joint stiffness: reciprocal activation and coactivation of antagonist muscles," *Adv Neurol*, vol. 39, pp. 347–372, 1983.

[29] A. E. Fiorilla, F. Nori, L. Masia, and G. Sandini, "Finger impedance evaluation by means of hand exoskeleton," *Annals of biomedical engineering*, vol. 39, no. 12, pp. 2945–2954, 2011.

[30] A. Z. Hajian and R. D. Howe, "Identification of the mechanical impedance at the human finger tip," *Journal of biomechanical engineering*, vol. 119, no. 1, pp. 109–114, 1997.

[31] H. Hoppner, D. Lakatos, H. Urbanek, C. Castellini, and P. van der Smagt, "The grasp perturbator: Calibrating human grasp stiffness during a graded force task," in *Robotics and Automation (ICRA), 2011 IEEE International Conference on.* IEEE, 2011, pp. 3312–3316.

[32] T. E. Milner and D. W. Franklin, "Characterization of multijoint finger stiffness: dependence on finger posture and force direction," *Biomedical Engineering, IEEE Transactions on*, vol. 45, no. 11, pp. 1363–1375, 1998.

[33] P. Buttolo, "Characterization of human pen grasp with haptic displays," Ph.D. dissertation, Citeseer, 1996.

[34] M. Bianchi, G. Grioli, E. P. Scilingo, M. Santello, and A. Bicchi, "Validation of a virtual reality environment to study anticipatory modulation of digit forces and position," in *Proceedings of the 2010 international conference on Haptics - generating and perceiving tangible sensations: Part II*, ser. EuroHaptics'10. Berlin, Heidelberg: Springer-Verlag, 2010, pp. 136–143.

[35] J. F. Soechting and M. Flanders, "Flexibility and repeatability of finger movements during typing: analysis of multiple degrees of

freedom," *Journal of computational neuroscience*, vol. 4, no. 1, pp. 29–46, 1997.

[36] M. Santello, M. Flanders, and J. F. Soechting, "Patterns of hand motion during grasping and the influence of sensory guidance," *The Journal of Neuroscience*, vol. 22, no. 4, pp. 1426–1435, 2002.

[37] R. Gentner and J. Classen, "Modular organization of finger movements by the human central nervous system," *Neuron*, vol. 52, no. 4, pp. 731–742, 2006.

[38] A. Bicchi, M. Gabiccini, and M. Santello, "Modelling natural and artificial hands with synergies," *Philosophical Transactions of the Royal Society B: Biological Sciences*, vol. 366, no. 1581, pp. 3153–3161, 2011.

[39] Z.-M. Li, M. Latash, and V. Zatsiorsky, "Force sharing among fingers as a model of the redundancy problem," *Experimental brain research*, vol. 119, no. 3, pp. 276–286, 1998.

[40] K. T. Reilly and G. R. Hammond, "Independence of force production by digits of the human hand," *Neuroscience letters*, vol. 290, no. 1, pp. 53–56, 2000.

[41] V. M. Zatsiorsky, Z.-M. Li, and M. L. Latash, "Enslaving effects in multi-finger force production," *Experimental brain research*, vol. 131, no. 2, pp. 187–195, 2000.

[42] S. L. Kilbreath and S. C. Gandevia, "Limited independent flexion of the thumb and fingers in human subjects," *J Physiol*, vol. 543, pp. 289 – 296, 2002.

[43] M. P. Rearick, A. Casares, and M. Santello, "Task-dependent modulation of multi-digit force coordination patterns," *Journal of neurophysiology*, vol. 89, no. 3, pp. 1317–1326, 2003.

[44] M. L. Latash, J. F. Scholz, F. Danion, and G. Schöner, "Structure of motor variability in marginally redundant multifinger force production tasks," *Experimental brain research*, vol. 141, no. 2, pp. 153–165, 2001.

[45] H. B. Olafsdottir, M. L. Latash, and V. M. Zatsisorsky, "Is the thumb a fifth finger?" *Studies of digit interaction during force production tasks*, 2005.

[46] F. Gao, S. Li, Z.-M. Li, M. L. Latash, and V. M. Zatsiorsky, "Matrix analyses of interaction among fingers in static force production tasks," *Biological cybernetics*, vol. 89, no. 6, pp. 407–414, 2003.

[47] J. P. Scholz and G. Schöner, "The uncontrolled manifold concept: identifying control variables for a functional task," *Experimental brain research*, vol. 126, no. 3, pp. 289–306, 1999.

[48] T. Iberall, G. Bingham, and M. Arbib, "Opposition space as a structuring concept for the analysis of skilled hand movements," *Experimental brain research series*, vol. 15, pp. 158–173, 1986.

[49] D. J. Ostry and A. G. Feldman, "A critical evaluation of the force control hypothesis in motor control," *Experimental Brain Research*, vol. 153, no. 3, pp. 275–288, 2003.

[50] J.-F. Pilon, S. J. De Serres, and A. G. Feldman, "Threshold position control of arm movement with anticipatory increase in grip force," *Experimental brain research*, vol. 181, no. 1, pp. 49–67, 2007.

[51] M. L. Latash, J. Friedman, S. W. Kim, A. G. Feldman, and V. M. Zatsiorsky, "Prehension synergies and control with referent hand configurations," *Experimental brain research*, vol. 202, no. 1, pp. 213–229, 2010.

[52] F. J. Valero-Cuevas, F. E. Zajac, and C. G. Burgar, "Large index-fingertip forces are produced by subject-independent patterns of muscle excitation," *Journal of biomechanics*, vol. 31, no. 8, pp. 693–703, 1998.

[53] F. J. Valero-Cuevas, "Predictive modulation of muscle coordination pattern magnitude scales fingertip force magnitude over the voluntary range," *Journal of Neurophysiology*, vol. 83, no. 3, pp. 1469–1479, 2000.

[54] A. Danna-Dos Santos, B. Poston, M. Jesunathadas, L. R. Bobich, T. M. Hamm, and M. Santello, "Influence of fatigue on hand muscle coordination and emg-emg coherence during three-digit grasping," *Journal of neurophysiology*, vol. 104, no. 6, pp. 3576–3587, 2010.

[55] B. Poston, A. Danna-Dos Santos, M. Jesunathadas, T. M. Hamm, and M. Santello, "Force-independent distribution of correlated neural inputs to hand muscles during three-digit grasping," *Journal of neurophysiology*, vol. 104, no. 2, pp. 1141–1154, 2010.

[56] E. J. Weiss and M. Flanders, "Muscular and postural synergies of the human hand," *Journal of Neurophysiology*, vol. 92, no. 1, pp. 523–535, 2004.

[57] F. J. Valero-Cuevas, M. Venkadesan, and E. Todorov, "Structured variability of muscle activations supports the minimal intervention principle of motor control," *Journal of neurophysiology*, vol. 102, no. 1, pp. 59–68, 2009.

[58] S. A. Winges and M. Santello, "Common input to motor units of digit flexors during multi-digit grasping," *Journal of neurophysiology*, vol. 92, no. 6, pp. 3210–3220, 2004.

[59] F. A. Mussa-Ivaldi, N. Hogan, and E. Bizzi, "Neural, mechanical, and geometric factors subserving arm posture in humans," *The Journal of neuroscience*, vol. 5, no. 10, pp. 2732–2743, 1985.

[60] T. Flash and F. Mussa-Ivaldi, "Human arm stiffness characteristics during the maintenance of posture," *Experimental brain research*, vol. 82, no. 2, pp. 315–326, 1990.

[61] T. Tsuji, P. G. Morasso, K. Goto, and K. Ito, "Human hand impedance characteristics during maintained posture," *Biological cybernetics*, vol. 72, no. 6, pp. 475–485, 1995.

[62] A. Ajoudani, N. G. Tsagarakis, and A. Bicchi, "Tele-Impedance: Teleoperation with impedance regulation using a body-machine interface," *International Journal of Robotics Research*, vol. 31(13), pp. 1642–1655, 2012.

[63] I. Kao, M. R. Cutkosky, and R. S. Johansson, "Robotic stiffness control and calibration as applied to human grasping tasks," *Robotics and Automation, IEEE Transactions on*, vol. 13, no. 4, pp. 557–566, 1997.

[64] C. L. Van Doren, "Grasp stiffness as a function of grasp force and finger span." *Motor control*, vol. 2, no. 4, pp. 352–378, 1998.

[65] J. Friedman and T. Flash, "Task-dependent selection of grasp kinematics and stiffness in human object manipulation," *Cortex*, vol. 43, no. 3, pp. 444–460, 2007.

[66] N. Hogan, "Impedance control: An approach to manipulation: Part ii?implementation," *Journal of dynamic systems, measurement, and control*, vol. 107, no. 1, pp. 8–16, 1985.

[67] S. J. Lederman and R. L. Klatzky, "Relative availability of surface and object properties during early haptic processing." *Journal of Experimental Psychology: Human perception and performance*, vol. 23, no. 6, p. 1680, 1997.

[68] P. Rochat, "Mouthing and grasping in neonates: Evidence for the early detection of what hard or soft substances afford for action,"

*Infant Behavior and Development*, vol. 10, no. 4, pp. 435–449, 1987.

[69] S. L. Gorniak, V. M. Zatsiorsky, and M. L. Latash, "Manipulation of a fragile object," *Experimental brain research*, vol. 202, no. 2, pp. 413–430, 2010.

[70] H. Hoppner, J. McIntyre, and P. van der Smagt, "Task dependency of grip stiffness. a study of human grip force and grip stiffness dependency during two different tasks with same grip forces," *PloS one*, vol. 8, no. 12, p. e80889, 2013.

[71] A. Serio, E. Riccomini, V. Tartaglia, I. Sarakoglou, M. Gabiccini, N. Tsagarakis, and A. Bicchi, "The patched intrinsic tactile object: a tool to investigate human grasps," 2014.

[72] J. M. Abu-Khalaf, J. W. Park, D. J. Mascaro, S. Mascaro *et al.*, "Stretchable fingernail sensors for measurement of fingertip force," in *EuroHaptics conference, 2009 and Symposium on Haptic Interfaces for Virtual Environment and Teleoperator Systems. World Haptics 2009. Third Joint.* IEEE, 2009, pp. 625–626.

[73] "Tekscan," https://www.tekscan.com.

[74] A. Bicchi, D. E. De Rossi, and E. P. Scilingo, "The role of the contact area spread rate in haptic discrimination of softness," *IEEE trans. on Robotics and Automation*, vol. 16, no. 5, pp. 496–504, October 2000.

[75] M. Bianchi, A. Serio, E. P. Scilingo, and A. Bicchi, "A new fabric based softness display," in *Symposium on Haptic Interfaces for Virtual Environments and Teleoperator Systems*, March 25-16 2010, pp. 108 – 112.

[76] A. Bicchi, J. K. Salisbury, and D. L. Brock, "Contact sensing from force measurements," *International Journal of Robotics Research*, vol. 12, no. 3, pp. 249–262, June 1993.

[77] C. Atkeson, C. An, and J. Hollerbach, "Rigid body load identification for manipulators," in *Decision and Control, 1985 24th IEEE Conference on*, Dec 1985, pp. 996–1002.

[78] D. Kubus, T. Kroger, and F. Wahl, "On-line rigid object recognition and pose estimation based on inertial parameters," in *Intelligent Robots and Systems, 2007. IROS 2007. IEEE/RSJ International Conference on*, Oct 2007, pp. 1402–1408.

[79] E. P. Scilingo, M. Bianchi, G. Grioli, and A. Bicchi, "Rendering softness: Integration of kinaesthetic and cutaneous information in a haptic device," *Transactions on Haptics*, vol. 3, no. 2, pp. 109 – 118, 2010.

[80] M. Kazemi, J.-S. Valois, J. A. Bagnell, and N. Pollard, "Human-inspired force compliant grasping primitives," *Autonomous Robots*, vol. 37, no. 2, pp. 209–225, 2014.

[81] M. A. Srinivasan and R. H. LaMotte, "Tactual discrimination of softness: abilities and mechanisms," in *Somesthesis and the Neurobiology of the Somatosensory Cortex*. Springer, 1996, pp. 123–135.

[82] E. Battaglia, G. Grioli, M. G. Catalano, M. Santello, and A. Bicchi, "Thimblesense: An individual-digit wearable tactile sensor for experimental grasp studies," in *Robotics and Automation (ICRA), 2014 IEEE International Conference on*, May 2014, pp. 2728–2735.

[83] S. L. Lederman and R. L. Klatzky, "Relative availability of surface and object properties during early haptic processing," *Journal of Experimental Psychology: Human Perception and Performance*, vol. 23, no. 6, pp. 1680–1707, December 1997.

[84] P. Space. Motion capture system. [Online]. Available: http://www.phasespace.com/

[85] D. W. Eggert, A. Lorusso, and R. B. Fisher, "Estimating 3-d rigid body transformations: a comparison of four major algorithms," *Machine Vision and Applications*, vol. 9, pp. 272 – 290, 1997.

[86] A. Bicchi, "On the problem of decomposing grasp and manipulation forces in multiple whole limb manipulation," *Int. Journal of Robotics and Autonomous Systems*, vol. 13, pp. 127 – 147, 1994.

[87] C. D. Meyer, *Matrix Analysis and Applied Linear Algebra*. Philadelphia, PA: Society for Industrial and Applied Mathematics, 2000.

[88] A. M. Smith, "The coactivation of antagonist muscles," *Canadian journal of physiology and pharmacology*, vol. 59, no. 7, pp. 733–747, 1981.

[89] M. Turvey, "Action and perception at the level of synergies," *Human Movement Science*, vol. 26, no. 4, pp. 657–697, 2007.

[90] M. Santello, M. Flanders, and J. Soechting, "Postural hand synergies for tool use," *The Journal of Neuroscience*, vol. 18, no. 23, pp. 10 105–10 115, 1998.

[91] A. Bicchi, M. Gabiccini, and M. Santello, "Modelling natural and artificial hands with synergies," *Philosophical Transactions of the Royal Society B: Biological Sciences*, vol. 366, no. 1581, pp. 3153–3161, 2011.

[92] A. Perotto and E. F. Delagi, *Anatomical guide for the electromyographer: the limbs and trunk*. Charles C Thomas Publisher, 2005.

[93] E. J. Perreault, R. F. Kirsch, and P. E. Crago, "Multijoint dynamics and postural stability of the human arm," *Experimental brain research*, vol. 157, no. 4, pp. 507–517, 2004.

[94] E. J. Perreault, R. F. Kirsch, and A. M. Acosta, "Multiple-input, multiple-output system identification for characterization of limb

stiffness dynamics," *Biological cybernetics*, vol. 80, no. 5, pp. 327–337, 1999.

[95] D. Shin, J. Kim, and Y. Koike, "A myokinetic arm model for estimating joint torque and stiffness from emg signals during maintained posture," *Journal of neurophysiology*, vol. 101, no. 1, pp. 387–401, 2009.